

Unhiding a concealed resonance by multiple Kondo transitions in a quantum dot

Aritra Lahiri,^{1,2} Tokuro Hata,³ Sergey Smirnov,⁴
Meydi Ferrier,^{3,5} Tomonori Arakawa,³ Michael Niklas,¹ Magdalena
Marganska,¹ Kensuke Kobayashi,^{3,6,7,*} and Milena Grifoni^{1,†}

¹*Institut für Theoretische Physik, Universität Regensburg, D-93040 Regensburg, Germany*

²*School of Physics and Astronomy, University of Minnesota, Minneapolis, MN 55455, USA*

³*Department of Physics, Graduate School of Science, Osaka University, 560-0043 Osaka, Japan*

⁴*P. N. Lebedev Physical Institute of the Russian Academy of Sciences, 119991 Moscow, Russia*

⁵*Laboratoire de Physique des Solides, CNRS, Univ. Paris-Sud,*

Université Paris Saclay, 91405 Orsay Cedex, France

⁶*Center for Spintronics Research Network (CSRN),*

Graduate School of Engineering Science, Osaka University, Osaka 560-8531, Japan

⁷*Institute for Physics of Intelligence and Department of Physics,*

The University of Tokyo, Tokyo 113-0033, Japan.

(Dated: October 26, 2021)

Kondo correlations are responsible for the emergence of a zero-bias peak in the low temperature differential conductance of Coulomb blockaded quantum dots. In the presence of a global $SU(2)\otimes SU(2)$ symmetry, which can be realized in carbon nanotubes, they also inhibit inelastic transitions which preserve the Kramers pseudospins associated to the symmetry. We report on magnetotransport experiments on a Kondo correlated carbon nanotube where resonant features at the bias corresponding to the pseudospin-preserving transitions are observed. We attribute this effect to a simultaneous enhancement of pseudospin-non-preserving transitions occurring at that bias. This process is boosted by asymmetric tunneling couplings of the two Kramers doublets to the leads and by asymmetries in the potential drops at the leads. Hence, the present work discloses a fundamental microscopic mechanisms ruling transport in Kondo systems far from equilibrium.

The Kondo effect [1] is a quintessential example of strong correlations in a many-body system, stemming from the screening of a localized spin by a Fermi sea of conduction electrons. Quantum dots (QD) in the Coulomb blockade regime, which effectively behave as a spin-1/2 system, provide a simple manifestation of $SU(2)$ Kondo entanglement between the dot spin and the lead conduction electrons, leading to the formation of a many-body spin singlet [2, 3]. The Kondo effect in QDs can also have more exotic realizations, provided that the associated degrees of freedom are conserved during tunneling. A prominent example are carbon nanotube (CNT) QDs where the presence of orbital (valley) and spin degrees of freedom leads to the $SU(4)$ [4–9] and the $SU(2)\otimes SU(2)$ Kondo effects [10–13]. The latter occurs when the valley and spin degeneracy of a CNT longitudinal mode is broken by spin-orbit coupling [14] or valley mixing [15], giving rise to two time-reversal protected Kramers doublets separated by an inter-Kramers splitting Δ , as seen in Fig. 1(a). A signature of the $SU(2)\otimes SU(2)$ Kondo effect is thus the occurrence of a zero-bias anomaly accompanied by two inelastic peaks, symmetrically located with respect to the central peak, in the differential conductance of a CNT with single electron or single hole occupancy [12]. Similar features are also seen in our experiment, as shown in Figs. 1(b), (c).

In analogy to the more conventional $SU(2)$ case, a pseudospin can be associated to each Kramers doublet of the CNT and the lead electrons [15]. While the central peak accounts for elastic virtual transitions which flip the

pseudospin of the CNT electron within the same Kramers doublet (\mathcal{T} -transition), the inelastic peaks denote transitions involving one state in the lower and one state in the upper Kramers doublet. One distinguishes between chiral (C) and particle-hole (P) transitions if the two states involve the opposite or the same pseudospin, respectively (see Fig. 2(a)). Strikingly, inelastic transitions of the P type are inhibited by effective anti-ferromagnetic exchange (Kondo) correlations between the pseudospins of lead and CNT electrons [15, 16], as confirmed by transport experiments at low magnetic fields [4, 6, 11–13]. However, P -transitions can be observed in the weak coupling regime, where Kondo correlations do not play a role and only lowest order cotunneling processes are responsible for the inelastic peaks [13, 17–19].

In this Letter, we demonstrate experimentally the puzzling emergence of a resonance at energies of the inelastic P -transition in Kondo correlated CNT QDs. Noticeably, the P -resonance is clearly seen only for a given bias polarity, suggesting its association with lead coupling asymmetries. We present a comprehensive theoretical analysis based on the Keldysh effective action (KEA) theory [12, 20], addressing the role of asymmetries in Kondo-correlated CNT QDs. The P -like features arise from the coherent addition of a C - and a \mathcal{T} -type transition, which occurs when the applied bias equals the energy of the inelastic P -transition, becoming relevant for different couplings of the Kramers doublets to the leads.

Experimental results.- Our device is made of a CNT grown by chemical vapour deposition and connected to

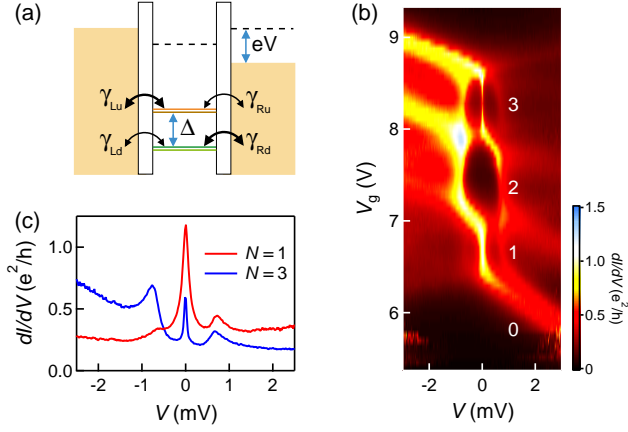


Figure 1: The $SU(2) \otimes SU(2)$ Kondo effect. a) A CNT longitudinal shell possesses two Kramer doublets separated by a splitting Δ . The upper (u) and lower (d) doublet are coupled to left (L) and right (R) leads by tunneling couplings γ_{Lp} and γ_{Rp} , where $p = u, d$. b) Experimental differential conductance as a function of gate, V_g , and bias, V , voltages for different occupation of a longitudinal shell. In the valleys with odd occupancy a zero-bias Kondo ridge is clearly seen. Two additional ridges, symmetrically located with respect to the central Kondo peak, are observed at finite bias. The asymmetric response implies the presence of asymmetries in the problem. c) Bias traces taken at gate voltages corresponding to the center of the $N = 1$ and $N = 3$ valleys show inelastic peaks with roughly the same spacing Δ .

Pd(6 nm)/Al(70 nm) leads. Fabrication details can be found in Ref. [8]. The differential conductance of our CNT QD is shown in Fig. 1(b) as a function of the applied bias V and gate voltage V_g . A small perpendicular magnetic field $B = 0.02$ T is applied to suppress superconductivity of Al in the leads. A Kondo ridge, corresponding to the yellow line at zero bias, is recognized in the Coulomb valleys with occupation $N = 1$ and $N = 3$ of a longitudinal shell. In the $N = 0, 2$ valleys, in contrast, no Kondo ridge is seen. Additional inelastic peaks, symmetrically located with respect to zero bias, are observed for the $N = 1, 2, 3$ valleys. Bias traces taken at gate voltages corresponding to the center of a valley are shown in Fig. 1(c). From such traces a Kramer splitting of $\Delta \simeq 0.7$ meV is estimated. Additionally, from the width of the zero-bias peaks Kondo temperatures of $T_{K1} = 1$ K and $T_{K3} = 0.37$ K are extracted for valley $N = 1$ and $N = 3$, respectively. Since our experiments are taken at temperatures around $T = 30$ mK, it holds $T < T_K$. Furthermore, from the evolution in perpendicular magnetic field (see Eq. (2) below), we can extract a spin-orbit coupling splitting $\Delta_{SO} = 0.07$ meV and a

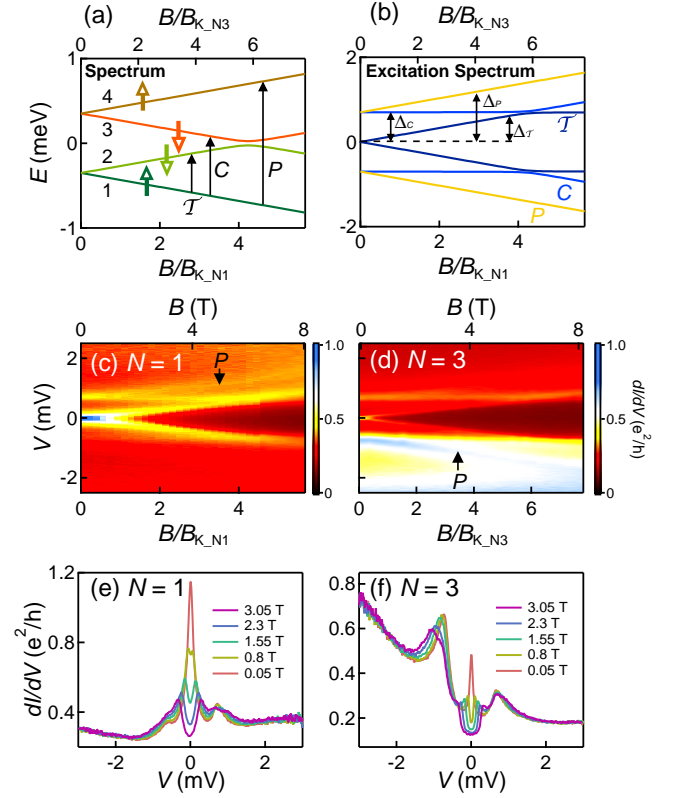


Figure 2: Behavior in perpendicular magnetic field. a) Evolution of energy levels in magnetic field; to each level is associated a Kramer pseudospin. b) Addition spectrum obtained from (a) with inelastic excitations Δ_T , Δ_C , and Δ_P associated to \mathcal{T} , \mathcal{C} and \mathcal{P} -transitions being indicated. The magnetic field is scaled by the characteristic fields $B_{K_{N1}} = 1.425$ T and $B_{K_{N3}} = 1.036$ T to emphasize universal behavior. c), d) Experimentally measured differential conductance vs scaled magnetic field. The \mathcal{P} -like resonances are clearly visible and indicated by an arrow. (e), (f) Experimental dI/dV vs bias voltage for various values of the magnetic field for (e) the one electron and (f) the three electron valley.

larger valley mixing energy $\Delta_{K,K'} = 0.7$ meV for both Kondo valleys.

A magnetic field breaks time-reversal symmetry and hence also Kramer degeneracy. The expected evolution of the single particle energy spectrum of a longitudinal shell and its associated excitation spectrum are shown in Figs. 2(a) and (b). The Kondo effect is however a many-body phenomenon, and differences in the excitation spectrum are expected. The experimental magnetoconductance is shown in Figs. 2(c) and (d); the reference field $B_K = eV_K/\mu_B$ is defined through the value V_K of the applied bias voltage where the low bias dif-

ferential conductance dI/dV is 2/3 of its value at zero-bias. This ensures universal behavior of the scaled magnetoconductance [21]. Differential conductance traces for different values of the magnetic field are shown in Figs. 2(e) and (f) and characterize the behavior at low fields. We find that the zero bias peak in valley $N = 1$ and $N = 3$ only splits above a critical field of the order of the reference field B_K , as expected from theoretical predictions [22, 23]. Further, the inelastic peaks do not split nor move at small values of the magnetic field for valley $N = 1$, suggesting a predominance of inelastic C -transitions [12, 13]. Valley $N = 3$ can be viewed as a shell with a single hole. Here the side peak at negative bias moves towards larger negative values of the bias voltage as the field increases, suggesting that a P -like transition is observed. Hence, the behavior is strongly asymmetric in the bias voltage and the P -like resonance is seen only for positive (negative) voltages for electron (hole) transport. In the following we propose a theoretical explanation for the experimental findings.

Model and KEA self-energy.- We consider the four-levels Anderson model to describe a longitudinal mode of a CNT quantum dot with both orbital and spin degrees of freedom. We denote by $|j\rangle$, $j = 1, \dots, 4$ the single-particle eigenstates and associate to the lower Kramers doublet the couple (1,2), to the upper the couple (3,4), see Fig. 2(a). The CNT Hamiltonian thus has the form

$$\hat{H}_{\text{CNT}} = \sum_j \varepsilon_j(B) \hat{n}_j + \frac{U}{2} \sum_{i \neq j} \hat{n}_i \hat{n}_j + \hat{H}_J, \quad (1)$$

where $\hat{n}_j = \hat{d}_j^\dagger \hat{d}_j$ is the occupation operator of level j , and $\varepsilon_{1,4}(B) = \varepsilon_d \mp \Delta(B)/2$, $\varepsilon_{2,3}(B) = \varepsilon_{1,4}(-B)$. Here

$$\Delta(B) = \sqrt{\Delta_{\text{SO}}^2 + (\Delta_{\text{K},\text{K}'} + g_s \mu_B B)^2} =: \Delta_P \quad (2)$$

is the magnetic field dependent level splitting ($g_s \mu_B$ is the spin magnetic moment). As indicated in the last equality, such level splitting yields the addition energy for the P -resonance. Finally, the second and third terms in Eq. (1) account for charging and exchange effects, respectively. We consider strong electron-electron interactions ($U = \infty$), such that double occupancy of the impurity is excluded and exchange effects are not relevant. The evolution of the four energy levels $\varepsilon_j(B)$ in magnetic field is shown in Fig. 2(a) together with the possible transitions (\mathcal{T} , \mathcal{C} , \mathcal{P}) from the ground state. The complete single-particle excitation spectrum is illustrated in Fig. 2(b). Notice that \mathcal{C} -excitations are independent of the magnetic field until the anticrossing of the inner levels (2,3). Further, it holds the relation $\Delta_P = \Delta_T + \Delta_C$, with $\Delta_T = \varepsilon_2 - \varepsilon_1 = \varepsilon_4 - \varepsilon_3$, and $\Delta_C = \varepsilon_3 - \varepsilon_1 = \varepsilon_4 - \varepsilon_2$.

Kondo correlations modify the simple single-particle picture, as shown in Figs. 2(c)-(f). To account for this behavior, we have evaluated the differential conductance of a four-levels Anderson model with bias and tunneling

asymmetries using the Keldysh effective action (KEA) method. Assuming that the Kramers degrees of freedom are conserved during tunneling [5, 16], KEA yields the tunneling density of states (TDOS) of channel j [12]

$$\nu_j(\varepsilon, B) = \frac{\Gamma/2\pi}{[\varepsilon_j(B) - \varepsilon + \Gamma_j \text{Re}\Sigma_j(\varepsilon, B)]^2 + [\Gamma_j \text{Im}\Sigma_j(\varepsilon, B)]^2}, \quad (3)$$

in terms of the KEA self-energies $\Sigma_j = \text{Re}\Sigma_j + i\text{Im}\Sigma_j$ being the central quantities of the theory. Here $\Gamma = \sum_{\alpha,j} \Gamma_{\alpha j}/4$ is the average coupling and $\Gamma_{\alpha j}$ are the tunneling couplings of channel j at lead $\alpha = L, R$. The current follows from the Meir and Wingreen formula [24]

$$I = \frac{e}{\hbar} \sum_{j=1}^4 \int_{-\infty}^{\infty} d\varepsilon \frac{\Gamma_{Lj} \Gamma_{Rj}}{\Gamma_{Lj} + \Gamma_{Rj}} \nu_j(\varepsilon) [f_L(\varepsilon) - f_R(\varepsilon)], \quad (4)$$

where $f_\alpha = [\exp \beta(\varepsilon - \mu_\alpha) + 1]^{-1}$ is the Fermi function, and $\mu_L = \mu_0 + \eta eV$, $\mu_R = \mu_0 - (1 - \eta)(eV)$ with $\eta \in [0, 1]$ accounting for an asymmetric bias drop between the left and right leads. The coupling asymmetry parameter for the lead α and level j is given by $\gamma_{\alpha j} = \Gamma_{\alpha j}/\Gamma_j$, with $\Gamma_j = \sum_\alpha \Gamma_{\alpha j}$. We keep the SU(2) symmetry within the same Kramers channel, and set

$$\gamma_{\alpha 1} = \gamma_{\alpha 2} := \gamma_{\alpha d}, \quad \gamma_{\alpha 3} = \gamma_{\alpha 4} := \gamma_{\alpha u}, \quad (5)$$

as illustrated in Fig. 1(a). Such asymmetries enter in the channel self-energies Σ_j , and hence impact the relevance of a given transition. For occupation $N = 1$ we find

$$\Sigma_j(\varepsilon, B) = \frac{1}{\pi} \sum_{i=T_j, C_j} \frac{\Gamma_i}{\Gamma_j} \left[\ln \left(\frac{W}{2\pi k_B T} \right) + \frac{i\pi}{2} - \sum_\alpha \gamma_{\alpha i} \Psi \left(\frac{1}{2} + \frac{\mathcal{E}}{2\pi k_B T} - i \frac{\mu_\alpha - \varepsilon + \Delta_{ji}}{2\pi k_B T} \right) \right], \quad (6)$$

where W is a high energy cut-off, Ψ is the digamma function, $\Delta_{ji} = \varepsilon_j - \varepsilon_i$, and T_j, C_j are the \mathcal{T} - and \mathcal{C} -partners of level j . The case $N = 3$ is obtained from Eq. (6) upon replacement of $\Delta_{ji} \rightarrow -\Delta_{ji}$. Finally, the complex quantity \mathcal{E} accounts for low energy contributions which make the self-energy finite also at zero temperature, as discussed in Sec. IV of the Supplemental Material.

Impact of asymmetries.- The analytic forms Eqs. (3), (4) allow us to analyze asymmetry effects on the differential conductance dI/dV . Before turning to highly nonequilibrium situations with $eV \simeq \Delta_P(B)$, we focus on low energies. An expansion of the zero temperature and zero magnetic field differential conductance G_{diff} in powers of the applied bias, $G_{\text{diff}} = G_0 + G_1 V + \dots$, yields

$$G_0 = \frac{2e^2}{h} \left[4\gamma_{Ld}\gamma_{Rd} + (\gamma_{Lu}\gamma_{Ru} - \gamma_{Ld}\gamma_{Rd}) \frac{\pi}{2} \Gamma_u \nu_u(\mu_0) \right], \quad (7)$$

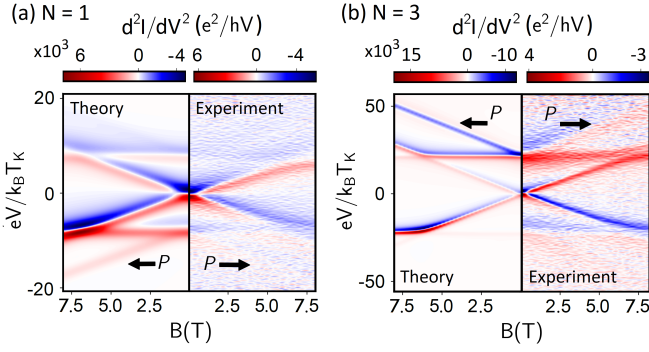


Figure 3: Second derivative of the current, d^2I/dV^2 , for the (a) $N = 1$ valley and, (b) $N = 3$ valley as a function of magnetic field. The left sub-panels show analytical predictions for the asymmetric four-level Anderson model, the right sub-panels the experimental observations. Kondo peaks in the differential conductance are manifested as zeros of d^2I/dV^2 as it changes from positive (red) to negative (blue) with increasing bias. Arrows point to the P -resonance.

being independent of the bias asymmetry η . The second term in the bracket is proportional to the transmission of the upper Kramers doublet at the Fermi level $\mathcal{T}_u(\mu_0) = \frac{\pi}{2}\Gamma_u\nu_u(\mu_0)$, and vanishes in the SU(4) coupling case where $\gamma_{au} = \gamma_{ad} = \gamma_\alpha$. Then Eq. (7) yields the known Fermi liquid result $G_0 = 4\gamma_L\gamma_R\frac{2e^2}{h}$. The expression for the linear term is lengthier and given in Sec. V of the Supplemental Material. Similar to G_0 , also G_1 is independent of the bias asymmetry η . Further, it is finite only in the presence of lead asymmetries encapsulated in the parameter $D_p = \gamma_{Lp} - \gamma_{Rp}$, $p = u, d$. For finite $D_u = D_d$ and $\Delta = 0$ we recover known results for the SU(4) case [25]. Here the linear term G_1 is non vanishing due to a small shift of the TDOS peak from the Fermi energy, as expected from the Friedel sum rule [26]. These results show that asymmetries can yield *qualitatively* different low energy behavior of a SU(2) \otimes SU(2) Kondo QD with respect to the symmetric case. Further, they suggest that the strong asymmetric behavior observed in the experimental data of Fig. 2 requires couplings $\gamma_{ad} \neq \gamma_{au}$.

Resonances at finite bias.— We start our analysis by showing in Fig. 3 KEA predictions for d^2I/dV^2 . The parameters $\Delta_{K,K'}$ and Δ_{SO} are obtained from Eq. (2) by a fit of the experimental magnetoconductance at large enough fields. The total linewidth Γ is extracted from a fit of the data near the charge peaks, as explained in the Supplemental Material. We fix $W/\Gamma = 100$; the remaining chosen set of free parameters is shown in Table I. As in the experiment, the KEA current-voltage characteristics display a P -peak at negative (positive) potential drop eV for valley $N = 1$ ($N = 3$).

To understand the origin of the resonance, we analyze

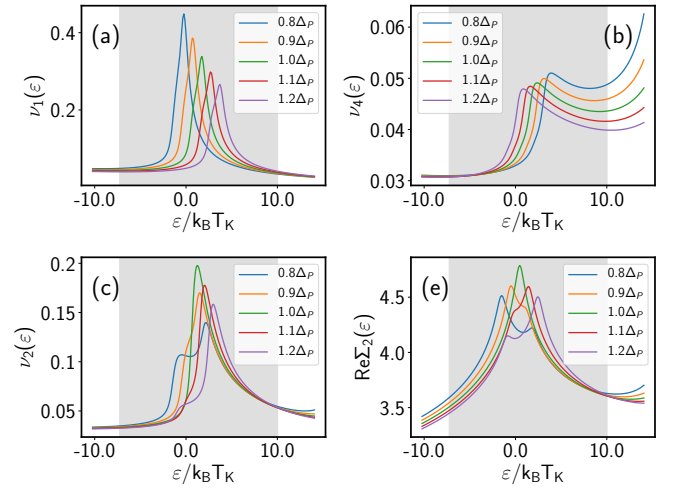


Figure 4: Channel density of states ν_j , (a)-(d), and self-energy Σ_2 of channel 2, panels (e) and (f), evaluated at bias drops $eV \simeq \Delta_P$, where Δ_P is the addition energy of the P -resonance, for the $N = 1$ case at $B = 8.05T$. The gray stripe indicates the bias window set by the lead chemical potentials when $eV = \Delta_P$. At $eV = \Delta_P$ the channel density of states ν_2 and ν_3 are maximal and of the order of ν_1 . This is due to a resonance of the associated self-energy, as illustrated in (e), (f) on the example of Σ_2 . On the other hand ν_4 is negligible.

each individual TDOS ν_j . In general, Kondo resonances appear in the differential conductance when a peak in one or more of the $\nu_j(\varepsilon)$ enters the bias window defined by $\mu_L - \mu_R = eV$. As seen from Eq. (6), the ν_j explicitly and significantly depend on the applied bias voltage through their self-energies Σ_j . Further, peaks in ν_j originate from peaks in $\text{Re}\Sigma_j$. At low temperatures, the latter occur when $\varepsilon = \mu_\alpha + \Delta_{ji} - \text{Im}\mathcal{E}$, with $i = T_j, C_j$. Simultaneously, $\text{Im}\Sigma_j$ drops by $\gamma_{\alpha i}$ as ε is swept across the resonance. Conventional Kondo resonances, i.e., the \mathcal{T} - and \mathcal{C} -resonances, arise as a consequence of a peak in ν_1 entering the bias window. The mechanism for the P -resonance is different.

In Fig. 4 we focus on the resonance in the $N = 1$ valley. We show the energy dependence of each $\nu_j(\varepsilon, eV)$ for different potential drops $eV \simeq \Delta(B) = \Delta_P$ for a magnetic field $B = 8.05T$. The gray region indicates the bias window for asymmetric potential drop $\eta = 0.4$ and $eV = \Delta_P$. From Figs. 4(a) and (b), we see that ν_1 is large while ν_4 is negligible in the integration window; further, ν_1 exhibits a monotonic variation as the potential drop increases. Strikingly, ν_2 and ν_3 develop a peak at $eV = \Delta_P$ and are of the same order of ν_1 , as seen in Figs. 4(c) and (d). The peak reflects a resonant feature of Σ_2 and Σ_3 , as shown in panels (e) and (f) on the example of Σ_2 . This occurs because when $\mu_L - \mu_R = \Delta_P (= \Delta_C + \Delta_T)$ the resonances of Σ_2 (Σ_3) at $\varepsilon = \mu_R + \Delta_T$ and $\varepsilon = \mu_L - \Delta_C$

TABLE I: Parameters used to fit the experimental data

N	Γ	$\mu_0 - \varepsilon_d$	γ_{Ld}	γ_{Lu}	η
1	3.5 meV	4.83	0.42	0.08	0.42
3	2.4 meV	5.36	0.3	0.06	0.1

($\varepsilon = \mu_R + \Delta_C$ and $\varepsilon = \mu_L - \Delta_T$) merge into a single concerted resonance. Correspondingly, the differential magnetoconductance displays a small resonance feature also at voltages matching the condition $eV = \Delta_P(B)$, as seen in Fig. 3. While the existence of this effect is independent of asymmetries, its magnitude does depend on them. Numerically, for $N = 1$ ($N = 3$) we find coupling asymmetry thresholds ζ_1 (ζ_3) above which the resonance is seen. E.g. for the valley $N = 1$ and $V < 0$ it should hold that $\gamma_{Lu} - \gamma_{Ld} > \zeta_1$. If the coupling strengths are reverted, $\gamma_{Ld} - \gamma_{Lu} > \zeta_1$, the resonance occurs at positive rather than at negative bias. Finally, the conditions for the single hole case, $N = 3$, can be obtained from the $N = 1$ case by replacing $u \leftrightarrow d$ and ζ_1 with ζ_3 . Thus, if a P -resonance is observed at positive bias in the $N = 1$ valley, it is likely that such resonance also occurs at negative bias in the $N = 3$ valley, in agreement with the experimental observations. Further, bias asymmetry may make it easier to observe a P -resonance for small values of $\mu_0 - \varepsilon_d$. The reason for this is that the tails from the charge-transfer peaks may assist the P -peaks if they are located at the same bias polarity. Since the asymmetry parameter η defines the bias window for the integration variable $\varepsilon \in [\mu_0 + \eta eV, \mu_0 - (1 - \eta)eV]$, P -peaks obtained at $\mu_L - \mu_R > 0$ are assisted by charge-transfer tails for $\eta < 0.5$, as seen in Fig. 1 and Fig. 2.

Note that virtual processes which involve a direct inelastic transition from the $j = 1$ to the $j = 4$ channel, namely a P -transition, are not explicitly appearing in the KEA self-energies Eq. (6). Pseudospin conserving cotunneling transitions become important at high temperatures and are the dominant contribution to P -like resonances outside the Kondo regime [13, 19].

Conclusion.- We have observed the emergence of inelastic resonances at bias voltages corresponding to pseudospin conserving P -transitions in a Kondo correlated CNT-QD. Due to the antiferromagnetic character of Kondo correlations, which inhibit direct P -transitions, these resonances emerge non trivially from a coherent addition of pseudospin non-conserving T - and C - transitions. The here established mechanism for P -like resonance becomes prominent in the presence of asymmetries in the tunneling coupling and bias drop.

A.L. and T.H. equally contributed to this work. We acknowledge support by the Deutsche Forschungsgemeinschaft within SFB 689, SFB 1277 B04, and by JSPS KAKENHI Grant Numbers JP15J01518, JP19H00656, and JP19H05826.

- * kensuke@meso.phys.sci.osaka-u.ac.jp
† milena.grifoni@physik.uni-regensburg.de
- [1] J. Kondo, Progress of Theoretical Physics **32**, 37 (1964).
 - [2] D. Goldhaber-Gordon, H. Shtrikman, D. Mahalu, D. Abusch-Magder, U. Meirav, and M. A. Kastner, Nature **391**, 156 (1998).
 - [3] S. M. Cronenwett, T. H. Oosterkamp, and L. P. Kouwenhoven, Science **281**, 540 (1998).
 - [4] P. Jarillo-Herrero, J. Kong, H. S. J. van der Zant, C. Dekker, L. P. Kouwenhoven, and S. De Franceschi, Nature **434**, 484 (2005).
 - [5] M.-S. Choi, R. López, and R. Aguado, Phys. Rev. Lett. **95**, 067204 (2005).
 - [6] A. Makarovski, J. Liu, and G. Finkelstein, Phys. Rev. Lett. **99**, 066801 (2007).
 - [7] F. Anders, D. Logan, M. Galpin, and G. Finkelstein, Phys. Rev. Lett. **100**, 086809 (2008).
 - [8] M. Ferrier, T. Arakawa, T. Hata, R. Fujiwara, R. Delagrè, R. Weil, R. Deblock, R. Sakano, A. Oguri, and K. Kobayashi, Nature Physics **12**, 230 (2016).
 - [9] M. Ferrier, T. Arakawa, T. Hata, R. Fujiwara, R. Delagrè, R. Deblock, Y. Teratani, R. Sakano, A. Oguri, and K. Kobayashi, Phys. Rev. Lett. **118**, 196803 (2017).
 - [10] T.-F. Fang, W. Zuo, and H.-G. Luo, Phys. Rev. Lett. **101**, 246805 (2008).
 - [11] J. P. Cleuziou, N. V. N'Guyen, S. Florens, and W. Wernsdorfer, Phys. Rev. Lett. **111**, 136803 (2013).
 - [12] D. R. Schmid, S. Smirnov, M. Margańska, A. Dirnacher, P. L. Stiller, M. Grifoni, A. K. Hüttel, and C. Strunk, Phys. Rev. B **91**, 155435 (2015).
 - [13] M. Niklas, S. Smirnov, D. Mantelli, M. Marganska, N.-V. Nguyen, W. Wernsdorfer, J.-P. Cleuziou, and M. Grifoni, Nature Communications **7**, 12442 (2016).
 - [14] M. R. Galpin, F. W. Jayatilaka, D. E. Logan, and F. B. Anders, Phys. Rev. B **81**, 075437 (2010).
 - [15] D. Mantelli, C. Moca, G. Zaránd, and M. Grifoni, Physica E **77**, 180 (2016).
 - [16] J. S. Lim, M.-S. Choi, M. Y. Choi, R. López, and R. Aguado, Phys. Rev. B **74**, 205119 (2006).
 - [17] J. Nygård, D. H. Cobden, and P. E. Lindelof, Nature **408** (2000).
 - [18] P. Jarillo-Herrero, J. Kong, H. S. J. van der Zant, C. Dekker, L. P. Kouwenhoven, and S. De Franceschi, Phys. Rev. Lett. **94**, 156802 (2005).
 - [19] T. Jespersen, K. Grove-Rasmussen, J. Paaske, K. Muraki, J. Nygård, and K. Flensberg, Nature Physics **7**, 348 (2011).
 - [20] S. Smirnov and M. Grifoni, Phys. Rev. B **87**, 121302 (2013).
 - [21] M. Gaass, A. K. Huettel, K. Kang, I. Weymann, J. von Delft, and C. Strunk, Phys. Rev. Lett. **107**, 176808 (2011).
 - [22] T. Costi, Phys. Rev. Lett. **85**, 1504 (2000).
 - [23] S. Smirnov and M. Grifoni, New J. Phys. **15**, 073047 (2013).
 - [24] Y. Meir and N. Wingreen, Phys. Rev. Lett. **68**, 2512 (1992).
 - [25] C. Mora, P. Vitushinsky, X. Leyronas, A. A. Clerk, and K. Le Hur, Phys. Rev. B **80**, 155322 (2009).
 - [26] A. C. Hewson, *The Kondo Problem to Heavy Fermions*, Cambridge Studies in Magnetism (Cambridge University

Press, 1993).

Supplementary Material: Unhiding a concealed resonance by multiple Kondo transitions in a quantum dot

Aritra Lahiri,^{1,2} Tokuro Hata,³ Sergey Smirnov,⁴
Meydi Ferrier,^{3,5} Tomonori Arakawa,³ Michael Niklas,¹ Magdalena
Marganska,¹ Kensuke Kobayashi,^{3,6,7,*} and Milena Grifoni^{1,†}

¹*Institut für Theoretische Physik, Universität Regensburg, D-93040 Regensburg, Germany*

²*School of Physics and Astronomy, University of Minnesota, Minneapolis, MN 55455, USA*

³*Department of Physics, Graduate School of Science, Osaka University, 560-0043 Osaka, Japan*

⁴*P. N. Lebedev Physical Institute of the Russian Academy of Sciences, 119991, Moscow, Russia*

⁵*Laboratoire de Physique des Solides, CNRS, Univ. Paris-Sud,*

Université Paris Saclay, 91405 Orsay Cedex, France

⁶*Center for Spintronics Research Network (CSRN),*

Graduate School of Engineering Science, Osaka University, Osaka 560-8531, Japan

⁷*Institute for Physics of Intelligence and Department of Physics,*

The University of Tokyo, Tokyo 113-0033, Japan.

(Dated: October 26, 2021)

CONTENTS

I. Model Hamiltonian	2
II. Tunneling density of states within the Keldysh effective action theory	3
III. Self-energies for perpendicular magnetic field	3
IV. Unitary conductance conditions	4
A. Constraints for the SU(4) case	6
B. Constraints for the SU(2)⊗SU(2) case	6
V. Low bias expansion of the differential conductance	8
A. The linear conductance G_0	9
B. The first order coefficient G_1	9
VI. Kondo transitions: TDOS and self-energy signatures	11
A. Self-energy resonances	11
B. P -transitions	12
C. Effect of tunneling coupling asymmetries	13
D. Bias drop asymmetries	14
VII. Matching between theory and experiment	15
A. Estimate of the ratio $(\mu_0 - \varepsilon_d)/\Gamma$	16
B. Contribution of the charge-transfer peaks to the Kondo resonances	16
1. $N = 3$	16
2. $N = 1$	17
C. Comparison: KEA theory and experiment	18
1. $N=1$	18
2. $N=3$	18
References	19

I. MODEL HAMILTONIAN

We describe a carbon nanotube (CNT) quantum dot in terms of a four-levels Anderson model, where the tunneling is diagonal in the Kramers basis, i.e. in the eigenbasis of the CNT. Then the Hamiltonian for the total leads-plus-CNT system reads

$$\hat{H}_{\text{tot}} = \sum_i \varepsilon_i(B) \hat{n}_i + U \sum_{i \neq j} \hat{n}_i \hat{n}_j + \sum_{\alpha, k, i} t_{\alpha i} \hat{c}_{\alpha i k}^\dagger \hat{d}_i + h.c. + \hat{H}_{\text{leads}}, \quad i, j = 1, \dots, 4 \quad (\text{S1})$$

where d_i/d_i^\dagger denote the dot electron operators for the i^{th} state, $\hat{n}_i = d_i^\dagger d_i$ is the occupation of the i^{th} state, U the charging energy. In the case of inter-Kramers splitting larger than the Kondo temperature, $\Delta > k_B T_K$, of relevance for the experiment, the distinct contribution from the two Kramers pairs must be considered. To properly describe this regime we set the single particle energies such that at zero magnetic field is $\varepsilon_{1,2} = \varepsilon_d$ for the lower Kramers pair and $\varepsilon_{3,4} = \varepsilon_u = \varepsilon_d + \Delta$ for the upper pair. Further, $c_{\alpha i k}/c_{\alpha i k}^\dagger$ denote the electron operators for the lead α characterized by the longitudinal wavevector k , and the index i . Finally, $t_{\alpha i}$ is the tunneling amplitude for tunneling from lead α in the i^{th} state. The resulting tunneling couplings are $\Gamma_{\alpha i} = 2\pi |t_{\alpha i}|^2 D(\varepsilon_F)$. Here $D(\varepsilon_F)$ is the lead density of states at the Fermi energy. For later convenience we introduce the normalized tunneling couplings $\gamma_{\alpha i} = \Gamma_{\alpha i} / \sum_{\alpha} \Gamma_{\alpha i}$.

We are interested in the Kondo effect in valley $N = 1$ and $N = 3$ of a CNT, corresponding to occupation with one electron or one hole, respectively. In this case it is sufficient to consider the limit of strong/infinite electron-electron interaction to capture the essential physics governing the Kondo effect in our system. In this limit, only virtual transitions to the empty dot state for valley $N = 1$, or the fully filled shell for valley $N = 3$, are included.

II. TUNNELING DENSITY OF STATES WITHIN THE KELDYSH EFFECTIVE ACTION THEORY

The current through our four-levels Anderson model is conveniently obtained from the tunneling density of states (TDOS) $\nu_j = -\frac{1}{\pi}\text{Im}G_j$ of level j according to the Meir and Wingreen formula¹⁻³, see Eq. (??) of the main text. Here $G_j(\varepsilon)$ is the Fourier transform of the retarded single particle Green's function $G_j(t) = -(i/\hbar)\theta(t)\langle\{c_i(t), c_i^\dagger\}\rangle$. The differential conductance $G_{\text{diff}} = \frac{d}{dV}I$ is in turn given by

$$G_{\text{diff}} = \frac{e^2}{\hbar} \frac{d}{d(eV)} \sum_{j=1}^4 \int_{-\infty}^{\infty} d\varepsilon \gamma_{Lj} \gamma_{Rj} \Gamma_j \nu_j(\varepsilon) [f_L(\varepsilon) - f_R(\varepsilon)]. \quad (\text{S2})$$

In this work the channel TDOS ν_j is evaluated along the lines of Ref. 4 using the method of the Keldysh effective action (KEA). Within the KEA, first an infinite- U slave boson transformation of the total Hamiltonian Eq. (S1) is performed. Then a functional field integral formulation is adopted for the problem (see Ref. 5, 6 for details). The functional integral approach is convenient as it enables one to integrate out the fermionic degrees of reservoirs and dot exactly, thus leaving an effective action which only depends on the bosonic field associated to the slave-boson operator. An expansion of the tunneling action about a non-zero slave-boson field configuration enables one to obtain an analytic expression for the TDOS. We find,

$$\nu_j(\varepsilon, \vec{B}) = \frac{1}{2\pi} \frac{\Gamma}{[\varepsilon_j(\vec{B}) - \varepsilon + \Gamma_j \text{Re}\Sigma_j(\varepsilon, \vec{B})]^2 + [\Gamma_j \text{Im}\Sigma_j(\varepsilon, \vec{B})]^2}, \quad (\text{S3})$$

where we explicitly indicated that ν_j may depend on an external magnetic field \vec{B} . Here $\Gamma_j = \sum_{\alpha} \Gamma_{\alpha j}$ and $\Gamma = (1/4) \sum_j \Gamma_j$ is the average rate. Furthermore, $\text{Re}\Sigma_j(\varepsilon, \vec{B})$ and $\text{Im}\Sigma_j(\varepsilon, \vec{B})$ are, respectively, the real and imaginary parts of the self-energy,

$$\Sigma_j(\varepsilon, \vec{B}) = - \sum_{\alpha} \sum_{i=1}^4 \gamma_{\alpha i} \frac{\Gamma_i}{\Gamma_j} \int_{-\infty}^{\infty} \frac{d\varepsilon'}{2\pi} \frac{L_W(\varepsilon') f_{\alpha}(\varepsilon')}{\varepsilon' - \varepsilon + \Delta_{ji}(\vec{B}) + iE_i^j}, \quad (\text{S4})$$

with $\Delta_{ji} = \varepsilon_j - \varepsilon_i$ the energy difference between the eigenstates j and i . Here $L_W(\varepsilon) = \frac{W^2}{\varepsilon^2 + W^2}$, with W being the lead bandwidth, cures ultraviolet divergences. Finally, the functions E_i^j are the product of the expansion points of the classical and quantum components of the slave-boson fields⁷, and are a crucial ingredient of the (KEA) theory to describe the non-perturbative unitary limit of the Kondo effect. Each of the E_i^j is not calculated *a priori*; instead, it is fixed by imposing *a posteriori* constraints on the channel TDOS. These are i) time-reversal and particle-hole conjugation relations which relate the TDOS component $\nu_j(\varepsilon, \vec{B})$ to its time-reversal and particle-hole related components; ii) the fulfillment of the Friedel sum rule⁸ with its implications. Such relations will be explicitly discussed in the next two sections.

III. SELF-ENERGIES FOR PERPENDICULAR MAGNETIC FIELD

In magnetic field the single particle energy levels ε_j acquire a magnetic field dependence. The splitting $\Delta(B) = \varepsilon_4(B) - \varepsilon_1(B) := \Delta_P$ is given explicitly in Eq. (??) of the main text for the case of a perpendicular magnetic field of magnitude B . Then one imposes the particle-hole and time-reversal conjugation relations

$$\begin{aligned} \nu_{1,2}(\varepsilon + \Delta(B)/2 - \varepsilon_M) &= \nu_{4,3}(\varepsilon - (\Delta(B)/2 - \varepsilon_M)), \\ \nu_{2,3}(\varepsilon, B) &= \nu_{1,4}(\varepsilon, -B), \end{aligned} \quad (\text{S5})$$

where $\varepsilon_M = \sum_j \varepsilon_j/4$ is the middle of the shell. This fixes some relations among the parameters E_i^j (cf. Eq. (B23) in Ref. 4), and leaves still just a parameter \mathcal{E} to be determined. Since in the Keldysh field integral the slave-bosonic fields $b(t)$ and $\bar{b}(t)$ are not complex conjugate of each other, the parameter \mathcal{E} must be complex. From the above equations also the chiral conjugation relations follow:

$$\nu_{1,2}(\varepsilon + \Delta(B)/2 - \varepsilon_M) = \nu_{3,4}(\varepsilon - (\Delta(-B)/2 - \varepsilon_M)). \quad (\text{S6})$$

Using such parametrization the equation for the self-energies Eq. (S4) turns into

$$\Sigma_j(\varepsilon, B) = \sum_{\alpha} \sum_{i=T_j, C_j} 2\gamma_{\alpha i} \frac{\Gamma_i}{\Gamma_j} K_{\alpha}(\varepsilon, \Delta_{ji}), \quad (\text{S7})$$

where we introduced the notation T_j, C_j for the states associated to the state j by time-reversal and chiral conjugation, respectively. Further,

$$K_\alpha(\varepsilon, \Delta) = - \int_{-\infty}^{\infty} \frac{d\varepsilon'}{2\pi} \frac{f_\alpha(\varepsilon') L_W(\varepsilon')}{\varepsilon' - \varepsilon + \Delta + i\varepsilon} = \frac{i}{4} + \frac{1}{2\pi} \left[\text{Re}\Psi\left(\frac{1}{2} + iz_\alpha\right) - \Psi\left(\frac{1}{2} + \frac{\mathcal{E}}{2\pi k_B T} - i\frac{\mu_\alpha - \varepsilon + \Delta}{2\pi k_B T}\right) \right], \quad (\text{S8})$$

where $\Psi(x)$ is the digamma function and $iz_\alpha = -(i\mu_\alpha + W)/2\pi k_B T$. Also, $\mu_\alpha = \mu_0 + eV_\alpha$, with $V_L - V_R = V$ the applied bias, are the lead electrochemical potentials. The complex function \mathcal{E} is now fully determined by the remaining requirements (set by the Friedel sum rule) to be fulfilled by the TDOS; the resulting equations for \mathcal{E} are explicitly derived in the next section.

In the limit of large cut-offs W the first digamma function in Eq. (S8) simplifies to $\text{Re}\Psi(1/2 + iz_\alpha) \approx \ln(W/2\pi k_B T)$, which is independent of the lead index α . From Eq. (S7) we thus find for the self-energies the form,

$$\Sigma_j(\varepsilon, B) = \frac{1}{\pi} \sum_{i=T_j, C_j} \frac{\Gamma_i}{\Gamma_j} \left[\ln\left(\frac{W}{2\pi k_B T}\right) + \frac{i\pi}{2} - \sum_\alpha \gamma_{\alpha i} \Psi\left(\frac{1}{2} + \frac{\mathcal{E}}{2\pi k_B T} - i\frac{\mu_\alpha - \varepsilon + \Delta_{ji}}{2\pi k_B T}\right) \right]. \quad (\text{S9})$$

This is Eq. (??) of the main text. We then find

$$\begin{aligned} \Gamma_j \text{Re}\Sigma_j(\varepsilon) &= \frac{1}{\pi} \sum_{i=T_j, C_j} \Gamma_i \left[\ln\left(\frac{W}{2\pi k_B T}\right) - \sum_\alpha \gamma_{\alpha i} \text{Re}\Psi\left(\frac{1}{2} + \frac{\mathcal{E}}{2\pi k_B T} - i\frac{\mu_\alpha - \varepsilon + \Delta_{ji}}{2\pi k_B T}\right) \right], \\ \Gamma_j \text{Im}\Sigma_j(\varepsilon) &= \frac{1}{\pi} \sum_{i=T_j, C_j} \Gamma_i \left[\frac{\pi}{2} - \sum_\alpha \gamma_{\alpha i} \text{Im}\Psi\left(\frac{1}{2} + \frac{\mathcal{E}}{2\pi k_B T} - i\frac{\mu_\alpha - \varepsilon + \Delta_{ji}}{2\pi k_B T}\right) \right]. \end{aligned} \quad (\text{S10})$$

IV. UNITARY CONDUCTANCE CONDITIONS

In this section we derive the equations that \mathcal{E} has to satisfy in the $SU(4)$ and $SU(2) \otimes SU(2)$ cases, reached for $k_B T_K \gg \Delta$ and $k_B T_K \leq \Delta$, respectively. Few relations involving the digamma functions listed below are required for the derivation.

$$\Psi\left(\frac{1}{2} + \frac{\mathcal{E}}{2\pi k_B T}\right) \Big|_{T \rightarrow 0} \approx \ln\left(\frac{\mathcal{E}}{2\pi k_B T}\right) + \frac{1}{24} \left(\frac{2\pi k_B T}{\mathcal{E}}\right)^2 \quad (\text{S11})$$

$$\implies T \frac{\partial}{\partial T} \Psi\left(\frac{1}{2} + \frac{\mathcal{E}}{2\pi k_B T}\right) \Big|_{T=0} = T \left(-\frac{d}{dT} \ln T + \frac{1}{24} \left(\frac{2T(2\pi k_B)}{\mathcal{E}}\right)^2 \right) \Big|_{T=0} = -1. \quad (\text{S12})$$

Further, the following chain relations hold

$$\frac{\partial}{\partial T} \Psi\left(\frac{1}{2} + \frac{\mathcal{E}}{2\pi k_B T} + \frac{i\varepsilon}{2\pi k_B T}\right) = \Psi\left(\frac{1}{2} + \frac{\mathcal{E}}{2\pi k_B T} + \frac{i\varepsilon}{2\pi k_B T}\right)' \left(-\frac{\mathcal{E} + i\varepsilon}{2\pi k_B T^2} \right), \quad (\text{S13})$$

$$\begin{aligned} \frac{\partial}{\partial \varepsilon} \Psi\left(\frac{1}{2} + \frac{\mathcal{E}}{2\pi k_B T} + \frac{i\varepsilon}{2\pi k_B T}\right) &= \Psi\left(\frac{1}{2} + \frac{\mathcal{E}}{2\pi k_B T} + \frac{i\varepsilon}{2\pi k_B T}\right)' \frac{i}{2\pi k_B T} \\ &= -\frac{i}{\mathcal{E} + i\varepsilon} T \frac{\partial}{\partial T} \Psi\left(\frac{1}{2} + \frac{\mathcal{E}}{2\pi k_B T} + \frac{i\varepsilon}{2\pi k_B T}\right). \end{aligned} \quad (\text{S14})$$

Therefore, using Eqns. (S13) and (S14),

$$\frac{\partial}{\partial \varepsilon} \Psi\left(\frac{1}{2} + \frac{\mathcal{E}}{2\pi k_B T} + \frac{i(\varepsilon - \mu_0)}{2\pi k_B T}\right) \Big|_{\substack{\varepsilon=\mu_0 \\ T=0}} = \frac{i}{\mathcal{E}} = \frac{\sin\varphi + i\cos\varphi}{|\mathcal{E}|}, \quad (\text{S15})$$

where we expressed $\mathcal{E} = |\mathcal{E}|e^{i\varphi}$. Similarly,

$$\frac{\partial^2}{\partial \varepsilon^2} \Psi\left(\frac{1}{2} + \frac{\mathcal{E}}{2\pi k_B T} + \frac{i(\varepsilon - \mu_0)}{2\pi k_B T}\right) \Big|_{\substack{\varepsilon=\mu_0 \\ T=0}} = \frac{\cos(2\varphi) - i\sin(2\varphi)}{|\mathcal{E}|^2}. \quad (\text{S16})$$

We are now in the position of fixing the real and imaginary parts of \mathcal{E} . To this extent we use the Friedel sum rule⁸. For the case of symmetrically coupled leads, $\gamma_{\alpha i} = 1/2$, it reads

$$\mathcal{T}_j(\mu_0) = \frac{\pi}{2} \Gamma_j \nu_j(\varepsilon_0) = \sin^2 \delta_j. \quad (\text{S17})$$

It relates the transmission per channel at the Fermi level $\mathcal{T}_j(\mu_0)$ to the scattering phase shift $\delta_j = \pi \langle n_j \rangle$, with $\langle n_j \rangle$ the average occupation of the level j . This in turn determines the zero temperature conductance through $G_0 = (e^2/h) \sum_j \mathcal{T}_j(\mu_0)$. The mean occupation depends on the energy degeneracy of a given channel. For example, in the SU(4) case with four-fold degeneracy and in the valley with $N = 1$ is $\langle n_j \rangle = 1/4$ for each $j = 1, \dots, 4$. As a consequence, $\mathcal{T}_j(\mu_0) = 1/2$ and $G_0 = 2e^2/h$ ⁹. Because the maximum value the transmission can take is one, this also means that the maximum of the transmission for the SU(4) does not lie at the Fermi level, but is actually shifted from it by a shift $\kappa \approx k_B T_K$. This shift is positive for $N = 1$ and negative for $N = 3$ ¹⁰.

For the SU(2) \otimes SU(2) case one needs the occupations of the lower and upper Kramers doublets $\langle n_{1,2} \rangle := \langle n_d \rangle$ and $\langle n_{3,4} \rangle := \langle n_u \rangle$, respectively. This yields the phase shifts $\delta_{u,d} = \pi \langle n_{u,d} \rangle$. When $\Delta \gg k_B T_K$ at zero temperature only the lower Kramers doublet will be occupied, $\langle n_d \rangle = 1/2$, with the upper being empty, $\langle n_{3,4} \rangle := \langle n_u \rangle = 0$. This yields $\mathcal{T}_{1,2}(\mu_0) = 1$, $\mathcal{T}_{3,4}(\mu_0) = 0$ and $G_0 = 2e^2/h$. As a consequence, matching the SU(2) behavior, the transmission is dominated by the lower Kramers doublet and is maximal at the Fermi level. For the intermediate case with $\Delta \approx k_B T_K$ the situation is more complex since both Kramers doublets are occupied. For generic Δ one can express the unbalance in the occupation between the lower and upper Kramers doublet in terms of the Kramers pseudospin magnetization δn defined by $\langle n_d \rangle = 1/4 + \delta n$ and $\langle n_u \rangle = 1/4 - \delta n$. Importantly, it still holds $\sin^2 \delta_d + \sin^2 \delta_u = 1$, which ensures $G_0 = 2e^2/h$ independent of the value of Δ ^{11,12}. On the other hand a finite polarization fixes the difference in the transmission at the Fermi level through $\sin^2 \delta_d - \sin^2 \delta_u = \sin(2\pi \delta n)$. The zero temperature equilibrium occupations $\langle n_{u,d} \rangle$ and hence δn can be evaluated exactly for generic Δ through the Bethe-Ansatz method¹¹. We postpone using proper Bethe-Ansatz equations for the determination of $\langle n_{u,d} \rangle$ to future analysis. Instead, here an approximation which accounts for the shifts and is appropriate for the parameter regime $\Delta > k_B T_K$ of our experiment will be discussed.

According to the above considerations,

- First we impose that in the limit of zero temperature, zero bias, zero magnetic field and for symmetric couplings the differential conductance of the CNT quantum dot reaches the correct unitary limit $G_0 = 2e^2/h$. The differential conductance $G_{\text{diff}} = \frac{d}{dV} I$ is given by (S2). In the symmetric case is $\gamma_{\alpha j} = 1/2$. It thus must hold

$$G_0 = \lim_{T, V, B \rightarrow 0} G_{\text{diff}} = \frac{e^2}{h} \sum_j \frac{\Gamma_j}{4} \nu_j(\varepsilon) \Big|_{\varepsilon=\mu_0} = \frac{2e^2}{h} \implies \frac{\pi}{2} (\Gamma_d \nu_d(\mu_0) + \Gamma_u \nu_u(\mu_0)) = 1, \quad (\text{S18})$$

where we set $\nu_{1,2} = \nu_d$ and $\nu_{3,4} = \nu_u$ for the TDOS of the lower and upper Kramers doublet, respectively.

To evaluate $\nu_j(\mu_0)$ we need the self-energies in this limit. From (S9) we get

$$\Sigma_j(\mu_0) = \frac{1}{\pi} \sum_{i=T_j, C_j} \frac{\Gamma_i}{\Gamma_j} \left[\ln \left(\frac{W}{2\pi k_B T} \right) + \frac{i\pi}{2} - \Psi \left(\frac{1}{2} + \frac{\mathcal{E}}{2\pi k_B T} - i \frac{\Delta_{ji}}{2\pi k_B T} \right) \right], \quad (\text{S19})$$

with contributions only from the chiral (C_j) and time-reversed (T_j) partners. The zero temperature channel TDOS are hence given by,

$$\nu_d(\mu_0) = \frac{\pi}{8\Gamma_d^2} \frac{\Gamma}{\left[\frac{(\varepsilon_d - \mu_0)\pi}{2\Gamma_d} + \frac{1}{2} \frac{\Gamma_u}{\Gamma_d} \ln \left(\frac{W}{|\mathcal{E} + i\Delta|} \right) + \frac{1}{2} \ln \left(\frac{W}{|\mathcal{E}|} \right) \right]^2 + \left[\frac{\pi}{4} \left(1 + \frac{\Gamma_u}{\Gamma_d} \right) - \frac{1}{2} \left(\varphi + \frac{\Gamma_u}{\Gamma_d} \varphi_+ \right) \right]^2}, \quad (\text{S20})$$

where $\varphi = \text{Arg}\{\mathcal{E}\}$, and $\varphi_+ = \text{Arg}\{\mathcal{E} + i\Delta\}$. Similarly,

$$\nu_u(\mu_0) = \frac{\pi}{8\Gamma_u^2} \frac{\Gamma}{\left[\frac{(\varepsilon_u - \mu_0)\pi}{2\Gamma_u} + \frac{1}{2} \frac{\Gamma_d}{\Gamma_u} \ln \left(\frac{W}{|\mathcal{E} - i\Delta|} \right) + \frac{1}{2} \ln \left(\frac{W}{|\mathcal{E}|} \right) \right]^2 + \left[\frac{\pi}{4} \left(1 + \frac{\Gamma_d}{\Gamma_u} \right) - \frac{1}{2} \left(\varphi + \frac{\Gamma_d}{\Gamma_u} \varphi_- \right) \right]^2}, \quad (\text{S21})$$

with $\varphi_- = \text{Arg}\{\mathcal{E} - i\Delta\}$.

- Second, we locate the peaks of the zero temperature and zero bias channel TDOS for the lower/upper Kramers channels appropriately. To this extent we introduce a parameter δ_j such that $\delta_j = \kappa_d$ if $j \in d$ and $\delta_j = \Delta + \kappa_u$ if $j \in u$. Further, for simplicity we approximate $\kappa_d \approx \kappa_u = \kappa$, and impose the condition

$$\left. \frac{d\nu_d}{d\varepsilon} \right|_{\substack{\varepsilon=\mu_0+\delta_d \\ V=T=0}} = 0, \quad \left. \frac{d\nu_u}{d\varepsilon} \right|_{\substack{\varepsilon=\mu_0+\delta_u \\ V=T=0}} = 0. \quad (\text{S22})$$

A. Constraints for the SU(4) case

The SU(4) case is characterized by fourfold degenerate levels, $\varepsilon_j = \varepsilon_d$, and by $\Gamma_j = \Gamma$. Hence for vanishing inter-Kramers splitting, $\Delta = 0$, one gets from Eq. (S20) the simpler SU(4) form

$$\nu_j(\mu_0) = \frac{\pi}{8\Gamma} \frac{1}{\left[\frac{(\varepsilon_d - \mu_0)\pi}{2\Gamma} + \ln\left(\frac{W}{|\mathcal{E}|}\right) \right]^2 + \left[\frac{\pi}{2} - \varphi \right]^2}, \quad (\text{S23})$$

being independent of j . We introduce now the SU(4) Kondo temperature $k_B T_K = 2W \exp(\pi(\varepsilon_d - \mu_0)/2\Gamma)$ to find

$$\nu_j(\mu_0) = \frac{\pi}{8\Gamma} \frac{1}{\left[\ln\left(\frac{k_B T_K}{2|\mathcal{E}|}\right) \right]^2 + \left[\frac{\pi}{2} - \varphi \right]^2}. \quad (\text{S24})$$

Thus, according to Eq. (S18), one finds the first condition on \mathcal{E} for the SU(4) case

$$\ln\left(\frac{2|\mathcal{E}|}{2k_B T_K}\right)^2 + \left[\frac{\pi}{2} - \varphi \right]^2 = \frac{\pi^2}{8}. \quad (\text{S25})$$

For the second condition we impose that $\nu_j(\varepsilon)$ has a peak at $\mu_0 + \kappa$ and notice that ν_j is independent of j in the SU(4) case. From the vanishing of the numerator N of the derivative of ν_j it follows

$$N = 2[(\varepsilon_d - \varepsilon) + \Gamma \text{Re}\Sigma(\varepsilon)] \left(-1 + \Gamma \frac{d\text{Re}\Sigma}{d\varepsilon} \right) \Big|_{\substack{\varepsilon=\mu_0+\kappa \\ V=0 \\ T=0}} + 2[\Gamma \text{Im}\Sigma] \left(\Gamma \frac{d\text{Im}\Sigma(\varepsilon)}{d\varepsilon} \right) \Big|_{\substack{\varepsilon=\mu_0+\kappa \\ V=0 \\ T=0}} = 0. \quad (\text{S26})$$

Hence, on using $\mathcal{E} + i\kappa = |\mathcal{E} + i\kappa| \exp\{i\varphi(\kappa)\}$, we find

$$\left[-\frac{\kappa\pi}{2\Gamma} - \ln\left(\frac{2|\mathcal{E} + i\kappa|}{k_B T_K}\right) \right] \left(\frac{\pi|\mathcal{E} + i\kappa|}{\Gamma} + 2\sin\varphi(\kappa) \right) + \left(\frac{\pi}{2} - \varphi(\kappa) \right) 2\cos\varphi(\kappa) = 0. \quad (\text{S27})$$

In summary, (S25) and (S27) together with the SU(4) shift $\kappa \approx k_B T_K$ determine the value $\mathcal{E}/k_B T_K$. These equations are universal. In contrast, the explicit value of T_K depends on microscopic details, like the actual values of $\mu_0 - \varepsilon_d$ and Γ .

B. Constraints for the SU(2)⊗SU(2) case

In the case of finite inter-Kramers splitting $\Delta > k_B T_K$, of relevance for the experiment, the distinct contribution from the two Kramers pairs must be considered. The Kondo temperature $T_K(\Delta)$ depends on Δ and one recovers the SU(4) one for vanishing splitting and equal couplings $\Gamma_j = \Gamma$. Further, $T_K(\Delta)$ decreases towards its smaller SU(2) value as Δ increases¹². In the SU(2)⊗SU(2) regime the conditions on \mathcal{E} are found along the lines followed for the degenerate SU(4) case. On the one hand the unitary condition (S18) is imposed, with ν_d and ν_u given by Eqs. (S20) and (S21), respectively. Further, as discussed above, a finite Δ requires in principle two distinct shifts κ_u and κ_d associated to the upper and lower Kramers pair, respectively¹¹. In the following we explicitly derive the constraints

imposed by Eq. (S22). Explicitly,

$$\begin{aligned}
\left. \frac{d\nu_j(\varepsilon)}{d\varepsilon} \right|_{\substack{\varepsilon=\mu_0+\delta_j \\ V=0 \\ T=0}} &= \left(\frac{-\Gamma}{2\pi} \right) \frac{\frac{d}{d\varepsilon} \left\{ [\varepsilon_j - \varepsilon + \Gamma_j \text{Re}\Sigma_j(\varepsilon)]^2 + [\Gamma_j \text{Im}\Sigma_j(\varepsilon)]^2 \right\}}{\left\{ [\varepsilon_j - \varepsilon + \Gamma_j \text{Re}\Sigma_j(\varepsilon)]^2 + [\Gamma_j \text{Im}\Sigma_j(\varepsilon)]^2 \right\}^2} \Big|_{\substack{\varepsilon=\mu_0+\delta_j \\ V=0 \\ T=0}} \\
&= \left(\frac{-2\Gamma}{2\pi} \right) \left(\frac{\pi^2}{4\Gamma_j^2} \right)^2 \frac{\left[\left(-1 + \Gamma_j \frac{d\text{Re}\Sigma_j(\varepsilon)}{d\varepsilon} \right) (\varepsilon_j - \varepsilon + \Gamma_j \text{Re}\Sigma_j(\varepsilon)) + \left(\Gamma_j \frac{d\text{Im}\Sigma_j(\varepsilon)}{d\varepsilon} \right) (\Gamma_j \text{Im}\Sigma_j(\varepsilon)) \right] \Big|_{\substack{\varepsilon=\mu_0+\delta_j \\ V=0 \\ T=0}}}{\left\{ \left[\left(\frac{\varepsilon_j - \mu_0 - \delta_j}{2\Gamma_j} \right) \pi + \frac{1}{2} \ln \left(\frac{W}{|\mathcal{E} + i\delta_j|} \right) + \frac{1}{2} \frac{\Gamma_{C_j}}{\Gamma_j} \ln \left(\frac{W}{|\mathcal{E} + i\delta_j - i\Delta_{j,C_j}|} \right) \right]^2 + \left[\frac{\pi}{4} \left(1 + \frac{\Gamma_{C_j}}{\Gamma_j} \right) - \frac{1}{2} \left(\varphi + \frac{\Gamma_{C_j}}{\Gamma_j} \frac{\varphi_{j,C_j}}{2} \right) \right]^2 \right\}^2}. \tag{S28}
\end{aligned}$$

It is convenient to introduce the abbreviations

$$\begin{aligned}
a_j(\mu_0 + \delta_j) &= \left. \frac{\pi}{2\Gamma_j} [\varepsilon_j - \varepsilon + \Gamma_j \text{Re}\Sigma_j(\varepsilon)] \right|_{\substack{\varepsilon=\mu_0+\delta_j \\ V=T=0}} = \left(\frac{\varepsilon_j - \mu_0 - \delta_j}{2\Gamma_j} \right) \pi + \frac{1}{2} \ln \left(\frac{W}{|\mathcal{E} + i\delta_j|} \right) + \frac{1}{2} \frac{\Gamma_{C_j}}{\Gamma_j} \ln \left(\frac{W}{|\mathcal{E} + i\delta_j - i\Delta_{j,C_j}|} \right), \\
b_j(\mu_0 + \delta_j) &= \left. \frac{\pi}{2\Gamma_j} \Gamma_j \text{Im}\Sigma_j(\varepsilon) \right|_{\substack{\varepsilon=\mu_0+\delta_j \\ V=T=0}} = \frac{\pi}{4} \left(1 + \frac{\Gamma_{C_j}}{\Gamma_j} \right) - \frac{1}{2} \left(\varphi + \frac{\Gamma_{C_j}}{\Gamma_j} \varphi_{j,C_j} \right). \tag{S29}
\end{aligned}$$

This yields the compact expression

$$\begin{aligned}
\left. \frac{d\nu_j(\varepsilon)}{d\varepsilon} \right|_{\substack{\varepsilon=\mu_0+\delta_j \\ V=0 \\ T=0}} &= -\frac{\Gamma}{\Gamma_j} \left(\frac{\pi}{2\Gamma_j} \right)^2 \frac{1}{(a_j^2(\mu_0 + \delta_j) + b_j^2(\mu_0 + \delta_j))^2} \\
&\times \left[a_j(\mu_0 + \delta_j) \left(-1 + \Gamma_j \frac{d\text{Re}\Sigma_j(\varepsilon)}{d\varepsilon} \Big|_{\substack{\varepsilon=\mu_0+\delta_j \\ V=0 \\ T=0}} \right) + b_j(\mu_0 + \delta_j) \left(\Gamma_j \frac{d\text{Im}\Sigma_j(\varepsilon)}{d\varepsilon} \Big|_{\substack{\varepsilon=\mu_0+\delta_j \\ V=0 \\ T=0}} \right) \right]. \tag{S30}
\end{aligned}$$

The derivative of $\text{Re}\Sigma$ is found along the same lines followed for Eq. (S15),

$$\begin{aligned}
\left. \frac{d\Sigma_j(\varepsilon)}{d\varepsilon} \right|_{\substack{\varepsilon=\mu_0+\delta_j \\ V=0 \\ T=0}} &= \frac{-1}{\pi} \left[\frac{d}{d\varepsilon} \Psi \left(\frac{1}{2} + \frac{\mathcal{E} - i(\mu_0 - \varepsilon)}{2\pi k_B T} \right) + \frac{\Gamma_{C_j}}{\Gamma_j} \frac{d}{d\varepsilon} \Psi \left(\frac{1}{2} + \frac{\mathcal{E} - i(\mu_0 - \varepsilon + \Delta_{j,C_j})}{2\pi k_B T} \right) \right] \Big|_{\substack{\varepsilon=\mu_0+\delta_j \\ T=0}} \\
&= \frac{-1}{\pi} \left[\frac{i\cos(\varphi(\delta_j)) + \sin(\varphi(\delta_j))}{|\mathcal{E} + i\delta_j|} + \frac{\Gamma_{C_j}}{\Gamma_j} \frac{i\cos(\varphi_{j,C_j}) + \sin(\varphi_{j,C_j})}{|\mathcal{E} + i\delta_j - i\Delta_{j,C_j}|} \right]. \tag{S31}
\end{aligned}$$

Notice that here is $\varphi_{j,C_j} = \varphi_{j,C_j}(\delta_j)$. Consequently,

$$\begin{aligned}
\left. \frac{d\nu_j(\varepsilon)}{d\varepsilon} \right|_{\substack{\varepsilon=\mu_0+\delta_j \\ V=0 \\ T=0}} &= \frac{\Gamma}{\Gamma_j} \frac{\pi}{4\Gamma_j} \left(\frac{1}{a_j^2(\mu_0 + \delta_j) + b_j^2(\mu_0 + \delta_j)} \right)^2 \\
&\times \left[a_j \left(\frac{\pi}{\Gamma_j} + \frac{\sin(\varphi(\delta_j))}{|\mathcal{E} + i\delta_j|} + \frac{\Gamma_{C_j}}{\Gamma_j} \frac{\sin(\varphi_{j,C_j})}{|\mathcal{E} + i\delta_j - i\Delta_{j,C_j}|} \right) + b_j \left(\frac{\cos(\varphi(\delta_j))}{|\mathcal{E} + i\delta_j|} + \frac{\Gamma_{C_j}}{\Gamma_j} \frac{\cos(\varphi_{j,C_j})}{|\mathcal{E} + i\delta_j - i\Delta_{j,C_j}|} \right) \right]. \tag{S32}
\end{aligned}$$

Finally, the peak of each TDOS is set appropriately according to Eq. (S22). Using now $\delta_{1,2} = \delta_d = \kappa$, $\delta_{3,4} = \delta_u = \Delta + \kappa$ we get the final conditions

$$\begin{aligned}
& a_d(\mu_0 + \kappa) \underbrace{\left(\frac{\pi}{\Gamma_d} + \frac{\sin(\varphi(\kappa))}{|\mathcal{E} + i\kappa|} + \frac{\Gamma_u \sin(\varphi_+(\kappa))}{\Gamma_d |\mathcal{E} + i\kappa + i\Delta|} \right)}_{\lambda_d(\kappa)} + b_d(\mu_0 + \kappa) \underbrace{\left(\frac{\cos(\varphi(\kappa))}{|\mathcal{E} + i\kappa|} + \frac{\Gamma_u \cos(\varphi_+(\kappa))}{\Gamma_d |\mathcal{E} + i\kappa + i\Delta|} \right)}_{\omega_d(\kappa)} = 0 \\
& a_u(\mu_0 + \Delta + \kappa) \underbrace{\left(\frac{\pi}{\Gamma_u} + \frac{\sin(\varphi_+(\kappa))}{|\mathcal{E} + i\Delta + i\kappa|} + \frac{\Gamma_d \sin(\varphi(\kappa))}{\Gamma_u |\mathcal{E} + i\kappa|} \right)}_{\lambda_u(\kappa)} + b_u(\mu_0 + \Delta + \kappa) \underbrace{\left(\frac{\cos(\varphi_+(\kappa))}{|\mathcal{E} + i\Delta + i\kappa|} + \frac{\Gamma_d \cos(\varphi(\kappa))}{\Gamma_u |\mathcal{E} + i\kappa|} \right)}_{\omega_u(\kappa)} = 0.
\end{aligned} \tag{S33}$$

Here we used $\Delta_{j,C_j} = \pm\Delta$ for $j \in u/d$, the upper/lower Kramers pair, and we introduced $\varphi_+(\kappa) = \text{Arg}(\mathcal{E} + i\Delta + i\kappa)$. The three equations (S18) and the pair given by (S33) are solved to yield $\text{Re}\mathcal{E}$, $\text{Im}\mathcal{E}$ and κ .

V. LOW BIAS EXPANSION OF THE DIFFERENTIAL CONDUCTANCE

To analyze the effect of the asymmetries on the low-bias behavior, a Taylor expansion of the differential conductance in the applied bias difference eV is sought:

$$G_{\text{diff}}(eV) = G_0 + G_1(eV) + \dots \tag{S34}$$

where $G_{\text{diff}} = e \frac{d}{d(eV)} I$ is given by Eq. (S2). The presence of a term linear in the applied bias signifies an asymmetric response. Along the lines of the previous section, we introduce the coefficients

$$a_j(\varepsilon, T, eV) = \frac{\pi(\varepsilon_j - \varepsilon)}{2\Gamma_j} + \frac{1}{2} \sum_{i=C_j, T_j} \frac{\Gamma_i}{\Gamma_j} \left[\ln \left(\frac{W}{2\pi k_B T} \right) - \sum_{\alpha=L,R} \gamma_{\alpha i} \text{Re}\Psi \left(\frac{1}{2} + \frac{\mathcal{E}}{2\pi k_B T} - \frac{i(\mu_\alpha - \varepsilon + \Delta_{ji})}{2\pi k_B T} \right) \right], \tag{S35}$$

$$b_j(\varepsilon, T, eV) = \frac{1}{2} \sum_{i=C_j, T_j} \frac{\Gamma_i}{\Gamma_j} \left[\frac{\pi}{2} - \sum_{\alpha=L,R} \sum_{i=C_j, T_j} \gamma_{\alpha i} \text{Im}\Psi \left(\frac{1}{2} + \frac{\mathcal{E}}{2\pi k_B T} - \frac{i(\mu_\alpha - \varepsilon + \Delta_{ji})}{2\pi k_B T} \right) \right], \tag{S36}$$

which permits one to write the channel TDOS in the compact form

$$\nu_j(\varepsilon) = \frac{\Gamma}{\Gamma_j} \frac{\pi}{8\Gamma_j} \frac{1}{a_j^2(\varepsilon) + b_j^2(\varepsilon)}. \tag{S37}$$

Introducing $g(\varepsilon) = \sum_j \frac{\Gamma}{\Gamma_j} \frac{\gamma_{Lj}\gamma_{Rj}}{a_j^2(\varepsilon) + b_j^2(\varepsilon)}$, we get the convenient expression

$$G_{\text{diff}} = \frac{e^2 \pi}{\hbar} \frac{d}{8 d(eV)} \int_{-\infty}^{\infty} d\varepsilon g(\varepsilon) [f_L(\varepsilon) - f_R(\varepsilon)]. \tag{S38}$$

The low bias expansion of the zero temperature differential conductance is thus,

$$\begin{aligned}
G_{\text{diff}} &= \frac{e^2 \pi}{\hbar} \frac{d}{8 d(eV)} \int_{\mu_R}^{\mu_L} d\varepsilon g(\varepsilon, T, eV) \\
&= \frac{e^2 \pi}{\hbar} \frac{d}{8} \left[\frac{d}{d(eV)} \int_{\mu_R}^{\mu_L} d\varepsilon g(\varepsilon, T, eV) \Big|_{\substack{V=0 \\ T=0}} + \frac{d^2}{d(eV)^2} \int_{\mu_R}^{\mu_L} d\varepsilon g(\varepsilon, T, eV) \Big|_{\substack{V=0 \\ T=0}} (eV) + \dots \right],
\end{aligned} \tag{S39}$$

where the temperature and bias dependence of the function g has been expressed explicitly.

A. The linear conductance G_0

Recalling $\mu_L = \mu_0 + \eta eV$ and $\mu_R = \mu_0 - (1 - \eta)eV$ it follows from Eq. (S39)

$$\begin{aligned} \frac{d}{d(eV)} \int_{\mu_0 - (1-\eta)eV}^{\mu_0 + \eta eV} d\varepsilon g(\varepsilon, T, eV) \Big|_{\substack{V=0 \\ T=0}} &= [g(\mu_0 + \eta eV, T, eV)\eta + g(\mu_0 - (1 - \eta)eV, T, eV)(1 - \eta)] \Big|_{\substack{V=0 \\ T=0}} \\ &+ \int_{\mu_0 - (1-\eta)eV}^{\mu_0 + \eta eV} d\varepsilon \frac{\partial g}{\partial(eV)}(\varepsilon, T, eV) \Big|_{\substack{V=0 \\ T=0}} = g(\mu_0, 0, 0). \end{aligned} \quad (\text{S40})$$

This yields $G_0 = \frac{e^2}{h} \frac{\pi^2}{4} g(\mu_0, 0, 0)$. We use the zero bias forms of the coefficients a_j and b_j , cf. Eqs. (S35) and (S36), as well as the unitarity condition (S18) found in the previous section. Then it follows for an $SU(2) \otimes SU(2)$ symmetric dot with lead coupling obeying $\gamma_{L1} = \gamma_{L2} = \gamma_{Ld}$ and $\gamma_{L3} = \gamma_{L4} = \gamma_{Lu}$,

$$\begin{aligned} G_0 &= \frac{2e^2}{h} \frac{\pi^2}{4} \frac{\Gamma}{\Gamma_d} \frac{\gamma_{Ld}\gamma_{Rd}}{\left[\frac{(\varepsilon_d - \mu_0)\pi}{2\Gamma_d} + \frac{1}{2} \left(\ln\left(\frac{W}{|\mathcal{E}|}\right) + \frac{\Gamma_u}{\Gamma_d} \ln\left(\frac{W}{|\mathcal{E} + i\Delta|}\right) \right) \right]^2 + \left[\frac{\pi}{4} \left(1 + \frac{\Gamma_u}{\Gamma_d} \right) - \frac{1}{2} \left(\varphi + \frac{\Gamma_u}{\Gamma_d} \varphi_+ \right) \right]^2} \\ &+ \frac{2e^2}{h} \frac{\pi^2}{4} \frac{\Gamma}{\Gamma_u} \frac{\gamma_{Lu}\gamma_{Ru}}{\left[\frac{(\varepsilon_u - \mu_0)\pi}{2\Gamma_u} + \frac{1}{2} \left(\ln\left(\frac{W}{|\mathcal{E}|}\right) + \frac{\Gamma_d}{\Gamma_u} \ln\left(\frac{W}{|\mathcal{E} - i\Delta|}\right) \right) \right]^2 + \left[\frac{\pi}{4} \left(1 + \frac{\Gamma_d}{\Gamma_u} \right) - \frac{1}{2} \left(\varphi + \frac{\Gamma_d}{\Gamma_u} \varphi_- \right) \right]^2} \end{aligned} \quad (\text{S41})$$

regardless of bias asymmetry. Using the unitary condition (S18) this simplifies to

$$G_0 = \frac{2e^2}{h} 4(\gamma_{Lu}\gamma_{Ru} - \gamma_{Ld}\gamma_{Rd}) \frac{\pi}{2} \Gamma_u \nu_u(\mu_0) + \frac{2e^2}{h} 4\gamma_{Ld}\gamma_{Rd}. \quad (\text{S42})$$

Notice that for the case of symmetric couplings, $\gamma_{\alpha i} = 1/2$ the value $G_0 = 2e^2/h$ is recovered. Further, for large values of Δ the upper channel TDOS vanishes and hence $G_0 \rightarrow \frac{2e^2}{h} 4\gamma_{Ld}\gamma_{Rd}$.

B. The first order coefficient G_1

We proceed with the evaluation of the coefficient G_1 in the expansion of the differential conductance G_{diff} . From (S39) we need

$$\begin{aligned} \frac{d^2}{d(eV)^2} \int_{\mu_0 - (1-\eta)eV}^{\mu_0 + \eta eV} d\varepsilon g(\varepsilon, T, eV) \Big|_{\substack{V=0 \\ T=0}} &= \left\{ \underbrace{\left[\eta \frac{d}{d(eV)} g(\mu_L, T, eV) + (1 - \eta) \frac{d}{d(eV)} g(\mu_R, T, eV) \right]}_A \right. \\ &+ \left. \underbrace{\left[\eta \frac{\partial}{\partial(eV)} g(\varepsilon, T, eV) \Big|_{\varepsilon=\mu_L} + (1 - \eta) \frac{\partial}{\partial(eV)} g(\varepsilon, T, eV) \Big|_{\varepsilon=\mu_R} \right]}_B + \underbrace{\int_{\mu_R}^{\mu_L} d\varepsilon \frac{\partial^2 g}{\partial(eV)^2}(\varepsilon, T, eV)}_C \right\} \Big|_{\substack{V=0 \\ T=0}}. \end{aligned} \quad (\text{S43})$$

The term C vanishes in the limit $V = 0$. For the remaining terms we introduce the voltage asymmetries $\eta_L = \eta$ and $\eta_R = -1 + \eta$. Further, we assign to the lead α the values $\alpha = L/R = \pm 1$. Then we get the compact forms

$$A = \sum_{\alpha} \alpha \eta_{\alpha} \frac{d}{d(eV)} g(\mu_{\alpha}, T, eV) \Big|_{\substack{V=0 \\ T=0}}, \quad B = \sum_{\alpha} \alpha \eta_{\alpha} \frac{\partial}{\partial(eV)} g(\varepsilon, T, eV) \Big|_{\substack{\varepsilon=\mu_{\alpha} \\ V=T=0}}. \quad (\text{S44})$$

We start by evaluating the term A , which involves total derivatives with respect to the bias voltage of the kind

$$\frac{d}{d(eV)} \frac{1}{a_j^2(\mu_{\alpha}, T, eV) + b_j^2(\mu_{\alpha}, T, eV)} = -2 \frac{a_j \frac{d}{d(eV)} a_j(\mu_{\alpha}, T, eV) + b_j \frac{d}{d(eV)} b_j(\mu_{\alpha}, T, eV)}{\left(a_j^2(\mu_{\alpha}, T, eV) + b_j^2(\mu_{\alpha}, T, eV) \right)^2}, \quad (\text{S45})$$

Using relation (S14) in the form

$$\frac{d}{d(eV)} \Psi \left(\frac{1}{2} + \frac{\mathcal{E} - i\Delta_{ji}}{2\pi k_B T} + i \frac{\mu_\alpha - \mu_\beta}{2\pi k_B T} \right) \Bigg|_{\substack{V=0 \\ T=0}} = i \frac{\eta_\alpha - \eta_\beta}{\mathcal{E} - i\Delta_{ji}}, \quad (\text{S46})$$

we find

$$\begin{aligned} \frac{d}{d(eV)} a_j(\mu_\alpha, T, eV) \Bigg|_{V=T=0} &= -\frac{\pi}{2\Gamma_j} \eta_\alpha - \frac{1}{2} \sum_{i=T_j, C_j} \frac{\Gamma_i}{\Gamma_j} \sum_{\beta} \gamma_{\beta i} \frac{\eta_\alpha - \eta_\beta}{|\mathcal{E} - i\Delta_{ji}|} \sin \varphi_{ji}, \\ \frac{d}{d(eV)} b_j(\mu_\alpha, T, eV) \Bigg|_{V=T=0} &= -\frac{1}{2} \sum_{i=T_j, C_j} \frac{\Gamma_i}{\Gamma_j} \sum_{\beta} \gamma_{\beta i} \frac{\eta_\alpha - \eta_\beta}{|\mathcal{E} - i\Delta_{ji}|} \cos \varphi_{ji}. \end{aligned} \quad (\text{S47})$$

Similarly, for the partial derivatives involved in the B term we obtain

$$\begin{aligned} \frac{\partial}{\partial(eV)} a_j(\varepsilon, T, eV) \Bigg|_{\substack{\varepsilon=\mu_\alpha \\ V=T=0}} &= -\frac{1}{2} \sum_{i=T_j, C_j} \frac{\Gamma_i}{\Gamma_j} \sum_{\beta} \gamma_{\beta i} \frac{(-\eta_\beta)}{|\mathcal{E} - i\Delta_{ji}|} \sin \varphi_{ji}, \\ \frac{\partial}{\partial(eV)} b_j(\mu_\alpha, T, eV) \Bigg|_{\substack{\varepsilon=\mu_\alpha \\ V=T=0}} &= -\frac{1}{2} \sum_{i=T_j, C_j} \frac{\Gamma_i}{\Gamma_j} \sum_{\beta} \gamma_{\beta i} \frac{(-\eta_\beta)}{|\mathcal{E} - i\Delta_{ji}|} \cos \varphi_{ji}. \end{aligned} \quad (\text{S48})$$

Notice that the above derivatives were calculated at zero bias and do not involve the shift κ . On using the relation

$$D_i \equiv \sum_{\alpha} \alpha \eta_{\alpha} \sum_{\beta} \gamma_{\beta i} (\eta_{\alpha} - 2\eta_{\beta}) = -\sum_{\beta} \beta \gamma_{\beta i} = \gamma_{Ri} - \gamma_{Li}, \quad (\text{S49})$$

we then obtain from Eqs. (S44) together with (S47) and (S48),

$$\begin{aligned} A + B &= \sum_j \frac{\Gamma}{\Gamma_j} \gamma_{Lj} \gamma_{Rj} \frac{(-2)}{\left(a_j^2(\mu_0, 0, 0) + b_j^2(\mu_0, 0, 0) \right)^2} \\ &\times \left\{ a_j(\mu_0, 0, 0) \left[-\frac{\pi}{2\Gamma_j} \sum_{\alpha} \eta_{\alpha} - \frac{1}{2} \sum_{i=T_j, C_j} \frac{\Gamma_i}{\Gamma_j} \frac{D_i}{|\mathcal{E} - i\Delta_{ji}|} \sin \varphi_{ji} \right] + b_j(\mu_0, 0, 0) \left[-\frac{1}{2} \sum_{i=T_j, C_j} \frac{\Gamma_i}{\Gamma_j} \frac{D_i}{|\mathcal{E} - i\Delta_{ji}|} \cos \varphi_{ji} \right] \right\}, \end{aligned} \quad (\text{S50})$$

from which $G_1 = \frac{e^2}{h} \frac{\pi}{8} (A + B)$ immediately follows. The contribution proportional to $a_j(\pi/2\Gamma_j) \sum_{\alpha} \eta_{\alpha}$ is usually neglected in the Kondo regime. As a result, G_1 becomes independent of the bias asymmetries η_{α} . Further, since $D_i = 0$ in a symmetric set up with $\gamma_{\beta i} = 1/2$, a non vanishing linear term G_1 requires that at least one $\gamma_{Li} \neq \gamma_{Ri}$. With the aim of revealing some key behaviours for $\Delta \gg k_B T_K$ in the crossover regime, we use that $a_d \ll a_u$ for large Δ . Then, we can approximate

$$\begin{aligned} G_1 &= \frac{e^2}{h} \frac{\pi}{4} \frac{\frac{\Gamma}{\Gamma_d} \gamma_{Ld} \gamma_{Rd}}{\left[a_d^2(\mu_0, 0, 0) + b_d^2(\mu_0, 0, 0) \right]^2} \left[(\gamma_{Rd} - \gamma_{Ld}) \left(a_d(\mu_0, 0, 0) \frac{\sin \varphi}{|\mathcal{E}|} + b_d(\mu_0, 0, 0) \frac{\cos \varphi}{|\mathcal{E}|} \right) \right. \\ &\quad \left. + (\gamma_{Lu} - \gamma_{Ru}) \left(a_d(\mu_0, 0, 0) \frac{\Gamma_u}{\Gamma_d} \frac{\cos \varphi_+}{|\mathcal{E} + i\Delta|} + b_d(\mu_0, 0, 0) \frac{\Gamma_u}{\Gamma_d} \frac{\cos \varphi_+}{|\mathcal{E} + i\Delta|} \right) \right] + \mathcal{O}((k_B T_K / \Delta)^4). \end{aligned} \quad (\text{S51})$$

Finally we turn to the SU(4) case, characterized by $\Delta = 0$, $\Gamma_j = \Gamma$, $a_j(\mu_0, 0, 0) = a$, $b_j(\mu_0, 0, 0) = b$, and $\gamma_{\alpha i} = \gamma_{\alpha}$. Then Eq. (S50) yields (upon neglecting the term proportional to a/Γ)

$$G_1 = \frac{2e^2}{h} \frac{\pi^2 \gamma_L \gamma_R (\gamma_R - \gamma_L)}{\left(a^2(\mu_0, 0, 0) + b^2(\mu_0, 0, 0) \right)^2} \left[-\ln \left(\frac{2|\mathcal{E}|}{k_B T_K} \right) \left(\frac{\sin \varphi}{|\mathcal{E}|} \right) + \left(\frac{\pi}{2} - \varphi \right) \left(\frac{\cos \varphi}{|\mathcal{E}|} \right) \right]. \quad (\text{S52})$$

Comparing the term in the bracket with the expression (S27), accounting for the shift κ of the location of the TDOS maximum from the energy μ_0 , we see that the two coincide if the shift κ is neglected. Thus, as a consequence of (S27), the term G_1 would vanish if the SU(4) shift κ is neglected. Lastly, the SU(2) case has no linear term irrespective of the asymmetries. Hence the zero-bias peak does not shift at all. The conclusions of our theory match that of Ref. 13.

VI. KONDO TRANSITIONS: TDOS AND SELF-ENERGY SIGNATURES

In this section we shortly review the mechanism leading to Kondo resonances.

A. Self-energy resonances

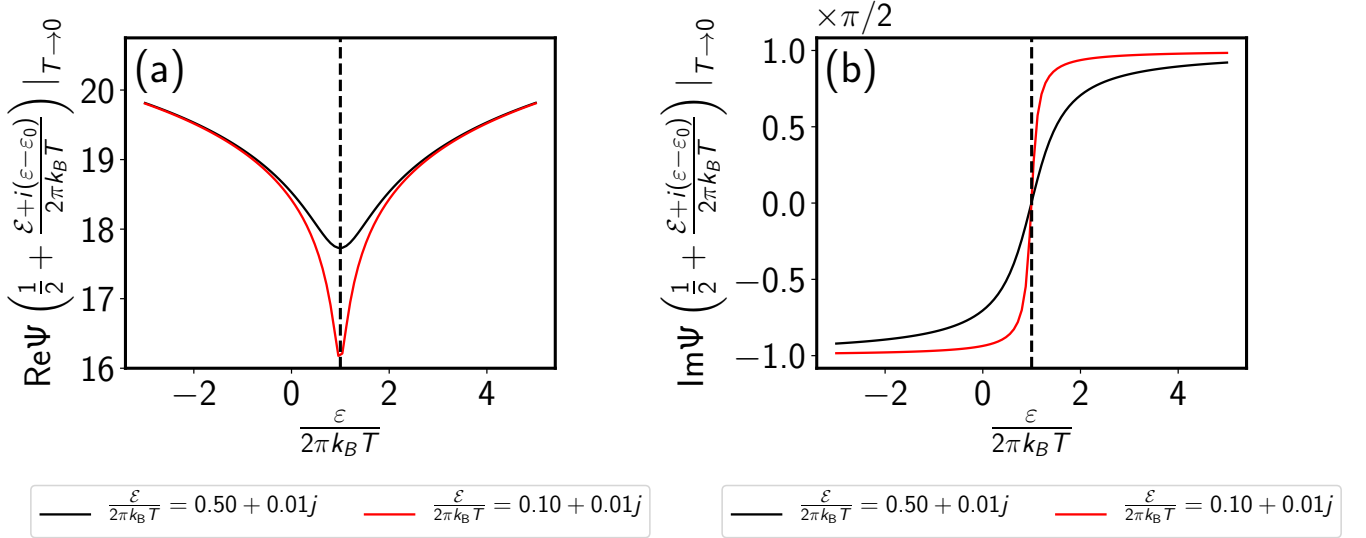
Since for the model considered in this work each channel j contributes independently to the current, it is sufficient to analyze the current per channel

$$I_j = \frac{e}{\hbar} \int_{-\infty}^{\infty} \frac{\Gamma_{L,j}\Gamma_{R,j}}{\Gamma_{L,j} + \Gamma_{R,j}} \nu_j(\varepsilon) (f_L(\varepsilon) - f_R(\varepsilon)) d\varepsilon. \quad (\text{S53})$$

Resonant features of the differential conductance $G_{\text{diff}} = \sum_j \frac{dI_j}{dV}$ are thus related to resonant features of the associated channel TDOS. From (S3), the denominator of the channel TDOS $\nu_j(\varepsilon)$ bears the form,

$$[(\varepsilon_j - \varepsilon) + \Gamma \text{Re}\Sigma_j(\varepsilon)]^2 + [\Gamma \text{Im}\Sigma_j(\varepsilon)]^2. \quad (\text{S54})$$

Thus, resonances are associated to values of the parameter ε which minimize the denominator (S54). Further, these values have to lie in the energy window set by the difference of Fermi functions in (S53). Hence, in the sequential tunneling regime where ε_j lies in the transport window (e.g. $\mu_L > \varepsilon_j > \mu_R$ for $eV > 0$), the TDOS has a peak at $\varepsilon = \varepsilon_j$, i.e. at the charge transfer peak. In the off-resonant regime, $\mu_L, \mu_R \gg \varepsilon_j$, the nature and number of resonances crucially depends on the energy dependence of the self-energy $\Sigma_j(\varepsilon)$, and in turn, according to (S9), on the energy dependence of digamma functions of the form $\Psi\left(\frac{1}{2} + \frac{\mathcal{E}}{2\pi k_B T} + i\frac{(\varepsilon - \varepsilon_0)}{2\pi k_B T}\right)$ ¹⁴. Such a behavior is shown in in Fig. S-1. The real part of the digamma function has a dip at $\varepsilon = \varepsilon_0 - \text{Im}\mathcal{E}$, and correspondingly the imaginary part has a change of π . We refer to these features henceforth as "resonant features". The sharpness of the peak and the abruptness of



Supplementary Figure S-1: Mechanism of resonances in the TDOS. Resonances in the Kondo regime are related to the low temperature behavior of the constituent digamma functions in the self-energies. These occur at $\varepsilon = \varepsilon_0 - \text{Im}\mathcal{E}$, where the real part has a dip while the imaginary part has a phase change of π . The resonance features are sharp for small $\mathcal{E}/2\pi k_B T$. For the simulation we choose $\varepsilon_0/2\pi k_B T = 1$, corresponding to the location of the vertical dashed line in panels (a) and (b).

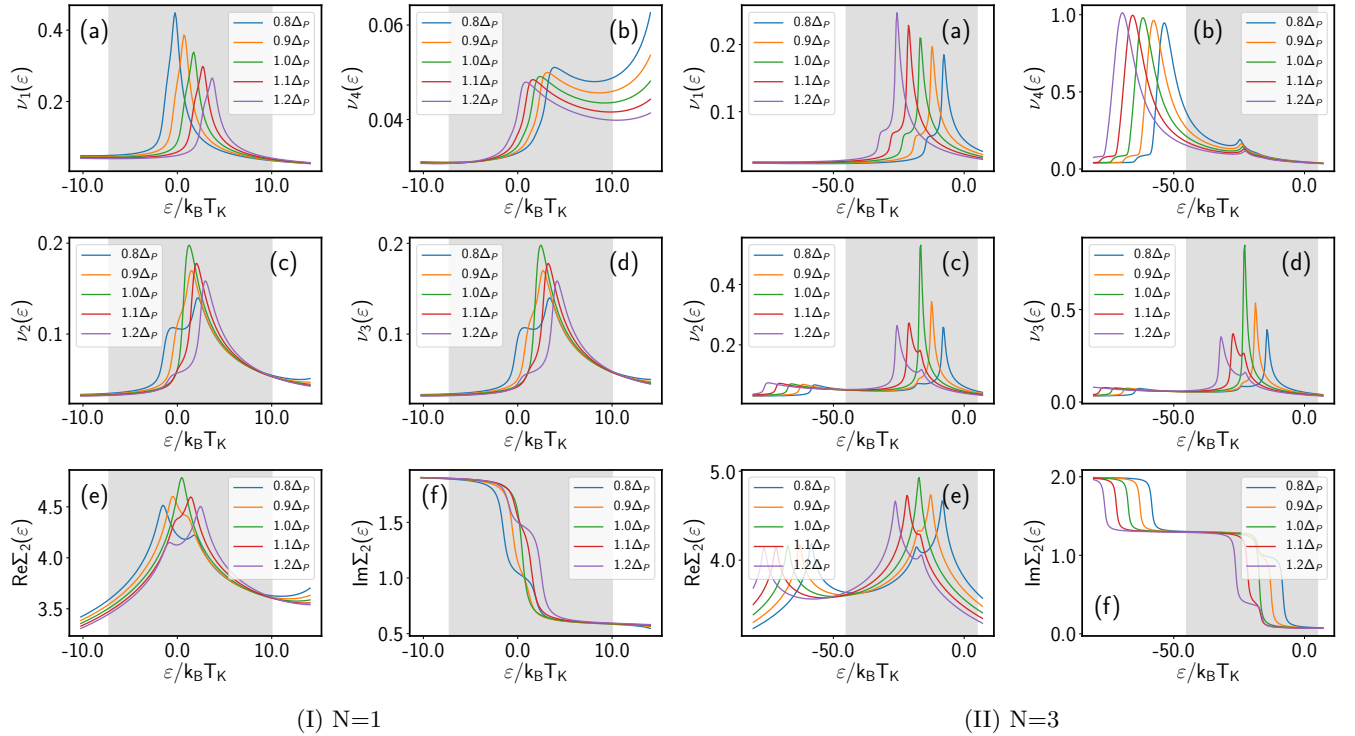
the sudden drop depend on the temperature $k_B T$ as well as on the magnitude of \mathcal{E} . For $T \rightarrow 0$, from Eq. (S11), a constituent digamma function in the self-energy Eq. (S9) is found to have the form,

$$\Psi\left(\frac{1}{2} + \frac{\mathcal{E}}{2\pi k_B T} + i\frac{(\varepsilon - \varepsilon_0)}{2\pi k_B T}\right) \xrightarrow{T \rightarrow 0} \ln\left(\frac{|\mathcal{E} + i(\varepsilon - \varepsilon_0)|}{2\pi k_B T}\right) + i \underbrace{\text{atan}\left(\frac{\text{Im}(\mathcal{E} + (\varepsilon - \varepsilon_0))}{\text{Re}(\mathcal{E})}\right)}_{\xrightarrow{\text{Re}\mathcal{E} \rightarrow 0} \text{sign}(\varepsilon - (\varepsilon_0 + \text{Im}\mathcal{E})) \frac{\pi}{2}} \quad (\text{S55})$$

which has a logarithmic dip in its real part at $\varepsilon = \varepsilon_0 - \text{Im}\mathcal{E}$, where the argument $|\mathcal{E} + i(\varepsilon - \varepsilon_0)|$ is the smallest, and a corresponding rise of π in its imaginary part. Additionally, at the tip of the dip, the real part assumes the value $\ln\left(\frac{\text{Re}\mathcal{E}}{2\pi k_B T}\right)$, while the width of the resonant feature is of the order of $\text{Re}\mathcal{E}$. Consequently, from Eqns. (S9) and (S55), it is clear that the real part of the self-energy exhibits a peak while the imaginary part has a sudden drop, leading to a Kondo peak in the TDOS. Further, a stronger peak in the real part and correspondingly, a sharper and/or larger drop in the imaginary part of the self-energies (i.e. stronger resonant feature), arising from a larger value of $\text{Re}\mathcal{E}$, leads to a stronger peak in the TDOS. Clearly, the strength of the Kondo resonances depend strongly on $\text{Re}\mathcal{E}$ while the location is slightly renormalized by $\text{Im}\mathcal{E}$.

B. P -transitions

From the above discussion and (S9) it follows that the digamma functions, and thus the associated self-energies, display Kondo resonances anytime $\varepsilon \approx \mu_\alpha + \Delta_{ji}$. This denotes a Kondo transition process between the levels $j \leftrightarrow i$ mediated by the lead α . In particular, as discussed in the main text, the resonances of the self-energy Σ_2 at $\varepsilon = \mu_R + \Delta_{21}$ and $\varepsilon = \mu_L + \Delta_{24}$ merge in a single resonance when the bias drop eV is such that $\mu_L - \mu_R = \Delta_{42} + \Delta_{21} = \Delta_{41} = \Delta_P$. Likewise for the self-energy Σ_3 . This effect was shown in Fig. 4 of the main text for the case of occupation $N = 1$. This behavior together with the one for occupation $N = 3$ is shown in S-2 for the same parameter set. In Fig. S-2, the channel tunneling density of states ν_j and the self-energy Σ_2 of the level two are



Supplementary Figure S-2: TDOS signatures of the P -resonance. Channel density of states ν_j , (a)-(d), and self-energy Σ_2 (e), (f), evaluated at bias drops around the energy Δ_P of the P -resonance, for the case $N = 1$, and $N = 3$ case. The gray stripe indicates the integration range set by the lead chemical potentials. At $eV = \Delta_P$ the channel density of states ν_2 and ν_3 are maximal. This is due to a resonance of the associated self-energy, as illustrated in (e), (f) on the example of Σ_2 . The magnetic field is $B = 8.05$ T, and we set $\Gamma_u = \Gamma_d = \Gamma$.

shown. Similar to the $N = 1$ case, the tunneling density of states ν_2 and ν_3 show a peak when the applied bias drop matches the energy Δ_P associated with the P -transition.

C. Effect of tunneling coupling asymmetries

From the above discussion it is clear that the condition for a P -resonance, $eV = \Delta_P$, is independent of the bias asymmetry η as well of the coupling asymmetries. However, the magnitude of the resonance, and hence whether the resonance is visible or not, is ruled also by asymmetries. For this we start looking at the role coupling asymmetries play in the magnitude of the drop of $\text{Im}\Sigma_2$ and $\text{Im}\Sigma_3$ at a P -transition. For clarity, let us consider the behavior of the self-energy Σ_2 . Further, we consider for simplicity the situation in which $\Gamma_u = \Gamma_d = \Gamma$. From (S9), we have that

$$\begin{aligned} \Sigma_2(\varepsilon) = & \frac{1}{\pi} \left[2 \ln \left(\frac{W}{2\pi k_B T} \right) + 2i \frac{\pi}{2} - \gamma_{Lu} \Psi \left(\frac{1}{2} + \frac{\mathcal{E}}{2\pi k_B T} - \frac{i\mu_L}{2\pi k_B T} + \frac{i\varepsilon}{2\pi k_B T} - \frac{i\Delta_{2,C_2}}{2\pi k_B T} \right) \right. \\ & - \gamma_{Ru} \Psi \left(\frac{1}{2} + \frac{\mathcal{E}}{2\pi k_B T} - \frac{i\mu_R}{2\pi k_B T} + \frac{i\varepsilon}{2\pi k_B T} - \frac{i\Delta_{2,C_2}}{2\pi k_B T} \right) - \gamma_{Ld} \Psi \left(\frac{1}{2} + \frac{\mathcal{E}}{2\pi k_B T} - \frac{i\mu_L}{2\pi k_B T} + \frac{i\varepsilon}{2\pi k_B T} - \frac{i\Delta_{2,T_2}}{2\pi k_B T} \right) \\ & \left. - \gamma_{Rd} \Psi \left(\frac{1}{2} + \frac{\mathcal{E}}{2\pi k_B T} - \frac{i\mu_R}{2\pi k_B T} + \frac{i\varepsilon}{2\pi k_B T} - \frac{i\Delta_{2,T_2}}{2\pi k_B T} \right) \right]. \end{aligned} \quad (\text{S56})$$

From the behavior of the digamma function as shown in Fig. S-1, it is clear that for very large negative values of ε is $\text{Im}\Sigma_2(\varepsilon) = 2$, see Fig. S-2. In fact, at zero temperature we have,

$$\lim_{\varepsilon \rightarrow -\infty} \text{Im}\Sigma_2(\varepsilon) = \frac{1}{\pi} \sum_{\alpha=L,R} \left[\frac{\pi}{2} + \gamma_{\alpha u} \frac{\pi}{2} + \gamma_{\alpha d} \frac{\pi}{2} \right] = \frac{1}{\pi} \left[2\frac{\pi}{2} + \frac{\pi}{2} + \frac{\pi}{2} \right] = 2. \quad (\text{S57})$$

At finite energies, there are four parameter configurations for which the self-energy shows resonant features. Namely, drops in $\text{Im}\Sigma_2$ are found at: $\varepsilon = \mu_R + \Delta_{2,C_2}$, $\mu_R + \Delta_{2,T_2}$, $\mu_L + \Delta_{2,C_2}$ and $\mu_L + \Delta_{2,T_2}$. Note that, for $\mu_L - \mu_R = \Delta_P$, regardless of the asymmetries, $\mu_L + \Delta_{2,C_2} = \mu_R + \Delta_{2,T_2}$, which is fundamental to the P -transitions. The first resonant feature is located at $\varepsilon = \mu_R + \Delta_{2,C_2}$ for $eV > 0$. We get

$$\text{Im}\Sigma_2(\varepsilon, 1st \text{ resonant feature crossed}) = 2 - \gamma_{Ru} = 1 + \gamma_{Lu}. \quad (\text{S58})$$

Similarly, after crossing three resonant features, barring the one located at the highest energy,

$$\text{Im}\Sigma_2(\varepsilon, 3rd \text{ resonant features crossed}) = 1 - \frac{1}{2} (\gamma_{Ru} + \gamma_{Rd} + \gamma_{Lu} - \gamma_{Ld}) = \gamma_{Ld}. \quad (\text{S59})$$

Therefore, when the resonant features corresponding to the T - and C -transitions merge, the height of the drop in $\text{Im}\Sigma_2(\varepsilon)$ is given by

$$\Delta \text{Im}\Sigma_2(\varepsilon, eV = \Delta_P) = 1 + \gamma_{Lu} - \gamma_{Ld}. \quad (\text{S60})$$

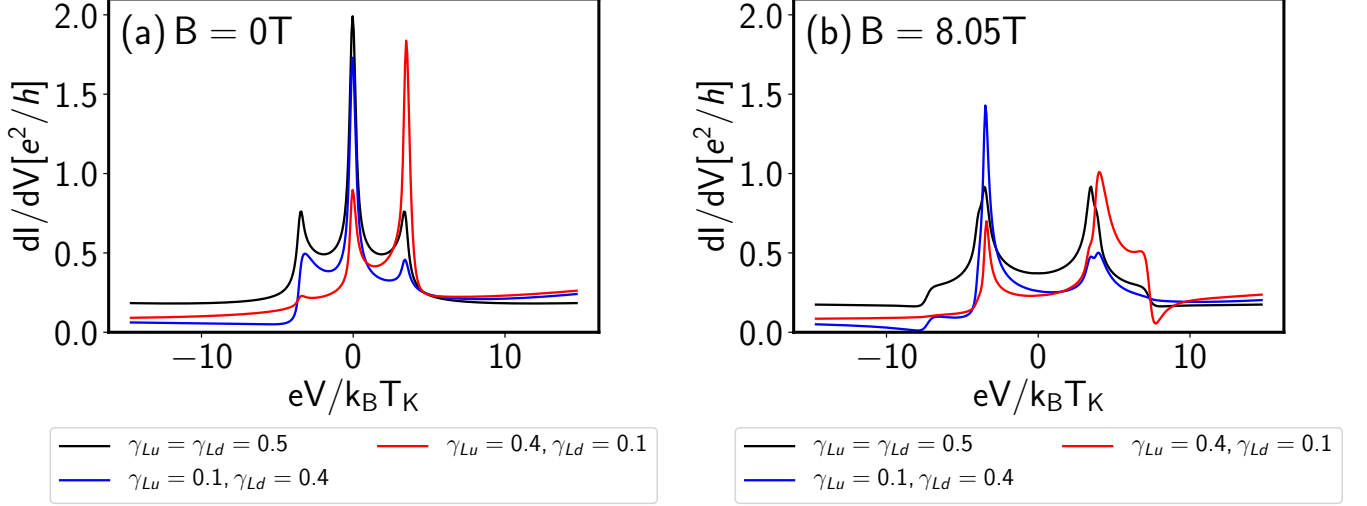
Clearly, this is directly dependent on the coupling asymmetry factors. Eqns. (S58) and (S59) may be verified by comparing with Fig. S-2(f). Further, when the upper Kramers pair is more strongly coupled to the left lead than the lower Kramers pair, i.e., $\gamma_{Lu} > \gamma_{Ld}$, then $\Delta \text{Im}\Sigma_2(\varepsilon, eV = \Delta_P)$ increases implying a stronger resonant feature. Consequently, from the discussion in Sec. VI, it is concluded that this strengthens the peak in the TDOS creating/strengthening the P -transition. Even though we can not give further analytical arguments, this suggests that a threshold value ζ_1 exists for the difference between γ_{Lu} and γ_{Ld} above which a P -resonance is seen. Now, one may repeat the derivation performed above using the self-energy expressions for both the $N = 1$ and $N = 3$ cases, along with $eV = \pm \Delta_P$. This yields the table below, describing the parameter domains for obtaining a P -transition. The small positive constants $\zeta_{1/3}$ represent threshold values for the magnitude of the coupling asymmetry required to yield a P -transition.

N	$\mu_L - \mu_R > 0$	$\mu_L - \mu_R < 0$
1	$\gamma_{Lu} - \gamma_{Ld} > \zeta_1$	$\gamma_{Ld} - \gamma_{Lu} > \zeta_1$
3	$\gamma_{Ld} - \gamma_{Lu} > \zeta_3$	$\gamma_{Lu} - \gamma_{Ld} > \zeta_3$

Supplementary Table I: The domains in the coupling asymmetry parameter space yielding a P -transition. Notice that $\zeta_{1/3} > 0$.

The impact of the tunneling coupling asymmetry on the P -transition is shown in Fig. S-3 for the $N = 1$ case. Fig. S-3(a) is taken as a reference as it shows the case of zero magnetic field which does not show a P -transition.

For Fig. S-3(b) a large value of the magnetic field, $B = 8.05$ T, is chosen. It is clear that equal tunnel couplings to both the Kramers pairs do not produce a P -transition. For the case $\gamma_{Lu} > \gamma_{Ld}$ and negative bias voltages the KEA theory yields a small peak at the position of the P -transition - with an adjacent dip - in the differential conductance. The dip is not seen in the experiment. We attribute this discrepancy to the lack of some cotunneling contributions in the KEA theory which can become relevant at high energies or to the strong impact of the Coulomb blockade peak which in the experiment might screen the dip.

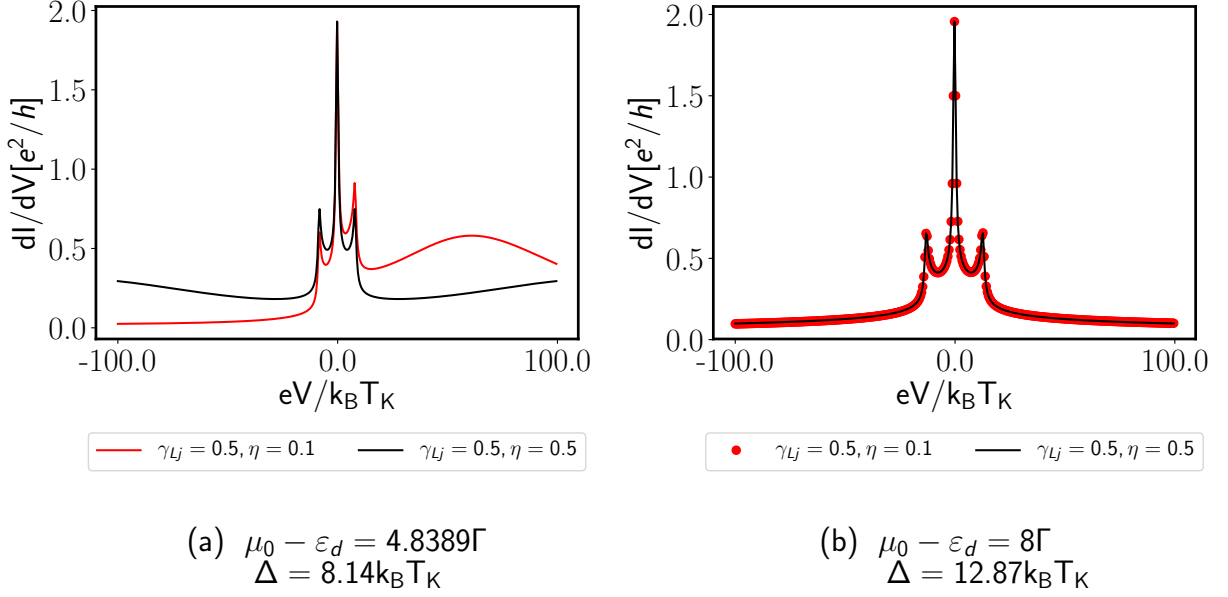


Supplementary Figure S-3: Differential conductance for the $N = 1$ case for (a) $B = 0$ T and (b) $B = 8.05$ T for various coupling asymmetries. The remaining parameters are the one used to match the $N = 1$ experimental data. The red curve in (b) with $\gamma_{Lu} > \gamma_{Ld}$ shows a P -transition at $\mu_L - \mu_R > 0$.

D. Bias drop asymmetries

Bias drop asymmetries have a much smaller and much less dramatic effect on the Kondo resonances compared to the coupling asymmetries as they primarily affect the high-energy/high-bias charge-transfer resonances. However, for a small value of $\mu_0 - \varepsilon_d$, the Lorentzian tails of the charge-transfer peaks may extend all the way to the low-bias/near zero-bias regime and skew the Kondo peak amplitudes, as seen in Fig. S-4(a). For larger differences the Kondo resonances remain untouched, as seen in Fig. S-4(b) where $\mu_0 - \varepsilon_d = 8\Gamma$ is chosen. Here, even in the presence of coupling asymmetries the bias asymmetries remain ineffective. This result can be understood by inspection of the self energy Σ_j and the associated channel TDOS ν_j . From (S9) the former may be written in the presence of bias asymmetries as (here for simplicity $\Gamma = \Gamma_i = \Gamma_u = \Gamma_d$ was chosen)

$$\begin{aligned}
\Sigma_j(\varepsilon) &= \frac{1}{\pi} \sum_{i=T_j, C_j} \left[\ln \left(\frac{W}{2\pi k_B T} \right) + i\frac{\pi}{2} - \gamma_{Li} \Psi \left(\frac{1}{2} + \frac{\varepsilon}{2\pi k_B T} - i \overbrace{\frac{eV/2 + (\eta - 1/2)eV - \varepsilon + \Delta_{ji}}{2\pi k_B T}}^{\mu_L} \right) \right. \\
&\quad \left. - \gamma_{Ri} \Psi \left(\frac{1}{2} + \frac{\varepsilon}{2\pi k_B T} - i \overbrace{\frac{-eV/2 + (\eta - 1/2)eV - \varepsilon + \Delta_{ji}}{2\pi k_B T}}^{\mu_R} \right) \right] \\
&= \frac{1}{\pi} \sum_{i=T_j, C_j} \left[\ln \left(\frac{W}{2\pi k_B T} \right) + i\frac{\pi}{2} - \gamma_{Li} \Psi \left(\frac{1}{2} + \frac{\varepsilon}{2\pi k_B T} - i \frac{\frac{eV}{2} - \varepsilon' + \Delta_{ji}}{2\pi k_B T} \right) \right. \\
&\quad \left. - \gamma_{Ri} \Psi \left(\frac{1}{2} + \frac{\varepsilon}{2\pi k_B T} - i \frac{-\frac{eV}{2} - \varepsilon' + \Delta_{ji}}{2\pi k_B T} \right) \right] := \Sigma_j^{\text{sym}}(\varepsilon'). \tag{S61}
\end{aligned}$$



Supplementary Figure S-4: Interplay of bias asymmetries and charge transfer peak on the differential conductance. The $N = 1$ case at $B = 0$ T is shown for two distinct values of the asymmetry parameter η for (a) $\mu_0 - \varepsilon_d = 4.8389\Gamma$, and (b) $\mu_0 - \varepsilon_d = 8\Gamma$. The remaining dot parameters are the ones used to match the $N = 1$ experimental data. Notice the negligible effect of bias asymmetries on the Kondo resonances for the parameter set in (b).

Here we have made the substitution $\varepsilon' = \varepsilon - (\eta - \frac{1}{2}) eV$, which recasts the self-energy in a bias-symmetric form without altering its features. In contrast, for the TDOS one finds from (S3) and (S61),

$$\begin{aligned}
 \nu_j(\varepsilon) &= \frac{1}{2\pi\Gamma_j} \frac{1}{\left(\frac{\varepsilon_j - \varepsilon}{\Gamma_j} + \text{Re}\Sigma_j(\varepsilon)\right)^2 + (\text{Im}\Sigma_j(\varepsilon))^2} \\
 &= \frac{1}{2\pi\Gamma_j} \frac{1}{\left(\frac{\varepsilon_j - \varepsilon'}{\Gamma_j} - \frac{(\eta - 1/2)eV}{\Gamma_j} + \text{Re}\Sigma_j^{\text{sym}}(\varepsilon')\right)^2 + (\text{Im}\Sigma_j^{\text{sym}}(\varepsilon'))^2}.
 \end{aligned} \tag{S62}$$

This shows that when the η -dependent contribution in the bracket can be neglected, as for the parameter set in Fig. S-4(b), the replacement $\varepsilon \rightarrow \varepsilon'$ just amounts to a rigid shift of the integration window which does not affect the differential conductance.

VII. MATCHING BETWEEN THEORY AND EXPERIMENT

From the experimental data it is possible to extract T_K , Γ and Δ . Specifically: i) The Kondo temperature $T_K(\Delta)$ is estimated from the width of the zero-bias peaks according to the approximate relation¹⁵ $G_{\text{diff}}(eV/k_B T_K(\Delta)) = (2/3)G_{\text{diff}}(eV = 0)$. We find $T_{K1} = 1$ K and $T_{K3} = 0.37$ K for valley $N = 1$ and $N = 3$, respectively. ii) The Kramers splitting $\Delta \simeq 0.7$ meV is extracted from the distance between the inelastic peaks of the differential conductance G_{diff} . iii) The average linewidth $\Gamma \simeq 2.44$ meV is extracted from a Lorentzian fit to the contribution of the charge transfer peaks, as discussed in subsection VII B below. This in turn yields an estimate for the ratios $k_B T_{K1}/\Gamma \simeq 0.025$, $k_B T_{K3}/\Gamma \simeq 0.013$.

Due to our assumption of infinite charging energy, $U \rightarrow \infty$, the theoretical Kondo temperature is given by

$$k_B T_K(\Delta) = f(\Delta) k_B T_K = f(\Delta) \left[2W \exp\left(-\pi \frac{(\mu_0 - \varepsilon_d)}{2\Gamma}\right) \right], \tag{S63}$$

where the ratio $(\mu_0 - \varepsilon_d)/\Gamma$ as well as the prefactor $f(\Delta)W$ cannot be directly extracted from the experiment. At low bias this is not important, since the relevant transport quantities show a universal behavior which is not affected by

bias and tunneling asymmetries, as seen in Fig. S-4. I.e., the experimentally measured and theoretically evaluated differential conductance collapse onto a universal curve when they are scaled by the respective Kondo temperatures. At larger bias, $|eV| \approx \Delta$, the charge transfer peak and the asymmetries may affect the differential conductance and thus a reasonable range of $(\mu_0 - \varepsilon_d)/\Gamma$ has to be chosen for the simulations as well. In our theory the bandwidth W is a free parameter. By fixing it to be $W/\Gamma = 100$, we find $\mu_0 - \varepsilon_d = 5.3643\Gamma$ using the procedure described in the following subsection VII A.

A. Estimate of the ratio $(\mu_0 - \varepsilon_d)/\Gamma$

Given the experimentally obtained values of the Kondo temperature T_K , of the splitting Δ , and of the tunnel coupling Γ , the calculation of $\varepsilon_d - \mu_0$ requires an iterative procedure. Since the prefactor $f(\Delta)$ in Eq. (S63) is unknown, we first fix W/Γ and then proceed iteratively:

- An initial value $f = f_1$ is assumed. By imposing $T_K(\text{theory}) = T_K(\text{experiment})$ a value for $(\mu_0 - \varepsilon_d)/\Gamma$ is found.
- Using these values and Δ , we find \mathcal{E} from the unitary conditions Eqns. (S18) and (S27).
- We obtain the Kondo temperature from the linear conductance using $G_0(T_K(\Delta)) = G_0(T = 0)/2$. This gives us $f = f_2$.
- Steps 2 and 3 are repeated until convergence for f .
- This value of f is used again in step 1 to get a new value for $\mu_0 - \varepsilon_d$.
- Steps 1-5 are repeated until convergence.

B. Contribution of the charge-transfer peaks to the Kondo resonances

We focus here on the resonant lines forming the borders of the Coulomb diamonds. Each of the lines corresponds to the electrochemical potential of the dot $\mu(N, V_g)$ being in resonance with either the source or the drain chemical potentials μ_L, μ_R . Thus, bias asymmetries impact the slopes of the lines. The strength of the resonance is instead governed by the coupling of the dot levels to the leads. From Fig. S-5(a), it is clear that either the bottom-right ($N = 1$ valley), or the top-left ($N = 3$ valley) edges harbor the strongest resonant lines. These lines correspond to the condition $\mu(1, V_g) = \mu_R$ and $\mu(3, V_g) = \mu_R$ and suggest a stronger coupling to the right lead.

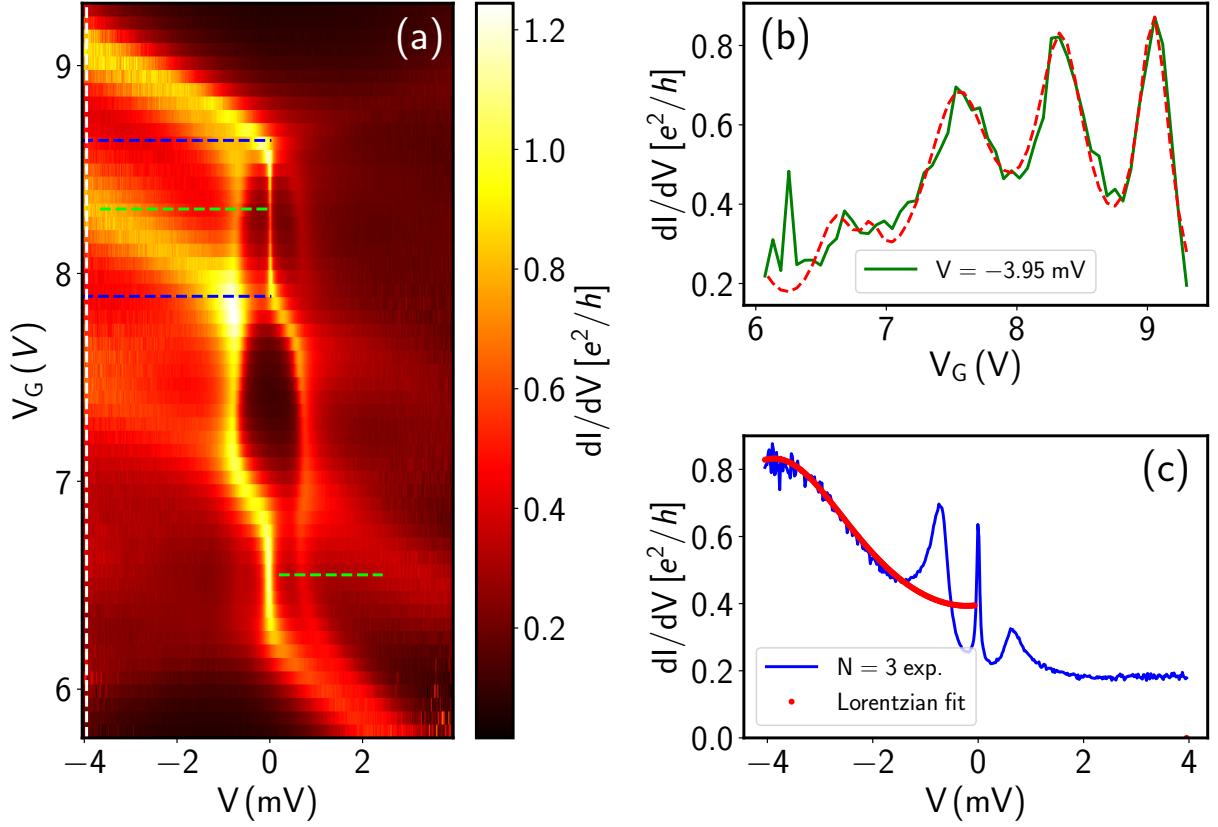
To extract the tunneling couplings we observe that we can fit gate traces near the resonance using a Breit-Wigner conductance formula which is applicable to Coulomb oscillations in the strong-coupling regime¹⁶. We hence approximate the differential conductance with respect to the gate voltage V_g by a sum of weighted Lorentzians, each corresponding to a Coulomb oscillation peak:

$$\left. \frac{dI}{dV} \right|_{\text{fit}}(V, V_g) = \frac{e^2}{h} \sum_l m_l \Gamma_l \frac{\Gamma_l}{\alpha_g^2 e^2 (V_g - c_l)^2 + \left(\frac{\Gamma_l}{2}\right)^2}. \quad (\text{S64})$$

Here m_l , c_l , and Γ_l are the weight, center, and FWHM of the Lorentzian fit of the l^{th} peak. Finally, α_g is the level arm accounting for the capacitive coupling to the gate voltage. The latter can be extracted by inspecting the $N = 3$ diamond of Fig. S-5(a). We start by estimating the charging energy U , which is given by the length of the green line in the $N = 3$ diamond. We obtain $\Delta V = U/e = 3.74$ mV. Likewise the separation ΔV_g of the blue lines bordering the $N = 3$ diamond gives the charging energy scaled by the gate capacitance factor α_g . Hence we obtain $\alpha_g = \frac{3.74 \text{ mV}}{0.75 \text{ V}} = 0.005$. Note that for a good fit of the gate trace to the data the low-bias regime must be avoided, to minimize contributions from the inelastic Kondo peaks.

1. $N = 3$

For the top-left border of Fig. S-5(a) ($N = 3$ valley) the analytical fitting of the experimental differential conductance is dominated by three Lorentzians originating from the resonances at the right lead, and is shown in Fig. S-5(b). The fitting parameters of the three dominant peaks are tabulated in Tab. II. In particular, the second Lorentzian has



Supplementary Figure S-5: Extracting the contribution from the charge transfer peaks. (a) Experimentally obtained dI/dV data. The green lines in valley $N = 1$, $N = 3$ mark the bias required to reach the border of the Coulomb diamond from the middle of the valley; the distance between the blue lines yields the addition energy corrected by the level arm α_g . (b) Lorentzian fit (red) of the experimental gate trace (green) at $V = -3.95$ mV. (c) Contribution to the differential conductance according to the Lorentzian fit (red dashed line) and experimental data (blue) as a function of the bias voltage.

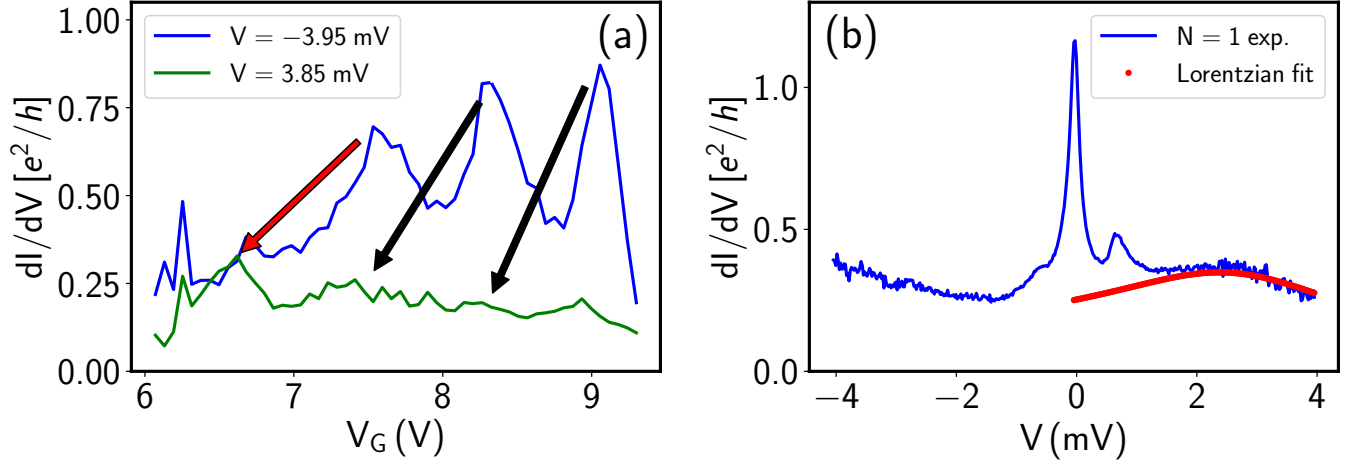
Peak (l)	Γ_l (meV)	m_l	c_l (V)
1	1.54	0.059	9.06
2	2.44	0.085	8.35
3	3.5	0.11	7.56

Supplementary Table II: Parameter set used for the fit of the three dominant peaks of the differential conductance for gate voltage ranges relevant for the $N = 3$ valley as shown in Fig. S-5(b).

$\Gamma_2 = 2.444$ meV. Since it is this charge transfer peak which most impacts the Kondo resonance, we approximate $\Gamma \approx \Gamma_2$. Together with $T_{K3} = 0.37$ K we find $\frac{k_B T_{K3}}{\Gamma} = 0.0131$. Finally, fixing $\frac{W}{\Gamma} = 100$, we get $\mu_0 - \varepsilon_d = 5.3643 \Gamma$ using the procedure described in Sec. VII A. As shown in Fig. S-5(c), the parameters extracted from the fitting can be used to evaluate the contribution to the differential conductance from the Coulomb peaks also as a function of the bias voltage. We notice that such contribution is quite remarkable and partly accounts for the different height of the inelastic Kondo peaks.

2. $N = 1$

The Lorentzian peak fitting is described and performed for the $N = 1$ case in Fig. S-6. The resonance line yielding the upper right edge of the $N = 1$ diamond in Fig. S-5(a), corresponding to $\mu(2) = \mu_R$, is the same line which yields



Supplementary Figure S-6: Lorentzian fit to the data for the $N = 1$ gate range. (a) Experimentally measured dI/dV at $V = 3.85$ mV (green) and $V = -3.95$ mV (blue). The Lorentzian fits to the experimental gate trace at positive bias are shown in red. The arrow marks the evolution of the charge-transfer peaks as the gate and bias voltages are varied. Notice that the peak belonging to the lower-left edge of the $N = 2$ Coulomb diamond evolves in the one belonging to the upper-right edge of the $N = 1$ Coulomb diamond (as marked by the red arrow). (b) The fitting parameters found in (a) are used in Eq. (S64) and extrapolated to find the differential conductance in the middle of the $N = 1$ Coulomb diamond over a range of bias voltages.

the peak indexed $l = 3$ in Tab. II at positive bias voltages. The line has the same linewidth $\Gamma_3 = 3.491$ meV but a diminished magnitude $m_3 = 0.06$. Hence, for the $N = 1$ case approximating $\Gamma \approx \Gamma_3$ and with $T_{K1} = 1$ K we find $\frac{k_B T_{K1}}{\Gamma} = 0.02487$. We choose $\frac{W}{\Gamma} = 100$, from which we get $\mu_0 - \varepsilon_d = 4.8389 \Gamma$ and $f(\Delta) = 0.4$ following the procedure described in Sec. VII A. Further, the Lorentzian fit can be used to estimate the impact of the Coulomb peaks on the differential conductance vs. bias, as seen in Fig. S-6(c). Notice that the fit cannot be extended all the way down to zero bias and beyond to the negative bias region as its validity is restricted to the edges of the Coulomb diamonds.

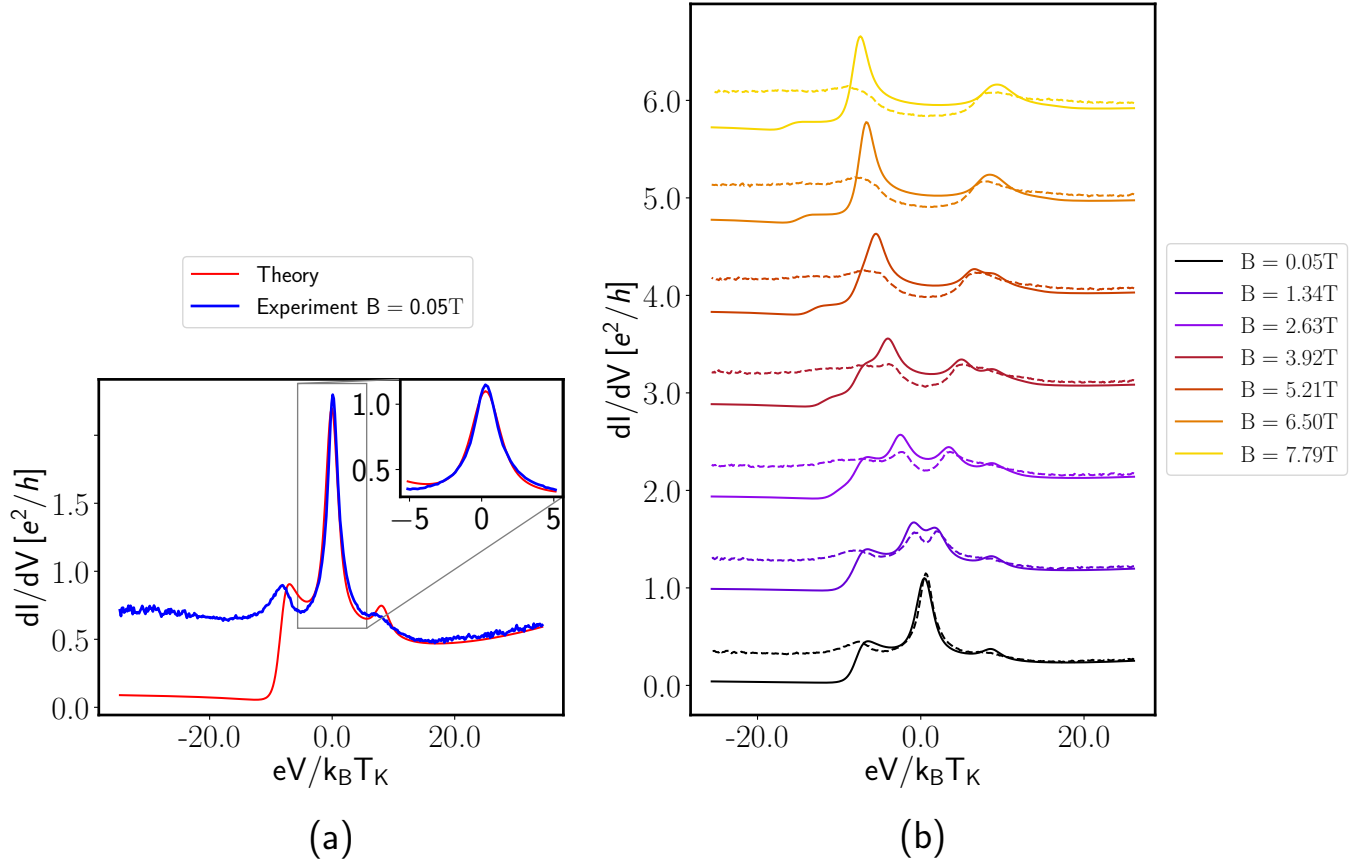
C. Comparison: KEA theory and experiment

1. $N=1$

The KEA results are compared with the experiment for the $N = 1$ case in Fig. S-7. Since the KEA assumes an infinite charging energy U , it cannot account for the contribution from the Coulomb line corresponding to the $\mu(2) = \mu_R$ resonance. Thus, the KEA calculation should be complemented with the Lorentzian fit discussed in the previous subsection, being of relevance at positive bias (or negative potential drop). On the other hand the KEA theory fully accounts for the Coulomb lines $\mu_\alpha = \mu(1)$ and hence properly describes the negative bias (positive potential drop) region. We notice that while the agreement between theory and experiment is reasonably good at small magnetic fields, it deteriorates as the field is increased. Also, the experimental data on that side is remarkably clear compared to the $N = 3$ case, where it is plagued by strong charge-transfer peak tails from the upper edges of the Coulomb diamond and other background conductance which is unaccounted for. In the positive bias region, the charge-transfer peak from the upper right edge of the $N = 1$ diamond leads to significant deviations between the experiment and our theory.

2. $N=3$

For the $N = 3$ case, the KEA results are matched with the experiments in Fig. S-8. The low-bias match is reasonably good, as seen in the inset in Fig. S-8(a). However, the high bias behavior shows a significant deviation between the experiment and the KEA theory. This may partly be attributed to the strong charge-transfer peak on the lower left edge of the $N = 3$ Coulomb diamond and a background conductance as seen in Fig. S-5(a). However, the location of the peaks of the differential conductance are well described by the KEA also at large magnetic fields.



Supplementary Figure S-7: Differential conductance for the $N = 1$ case, at (a) $B = 0.05$ T and (b) for various values of the magnetic field. The blue curve in (a) shows the experimental trace while the red one shows the results of the KEA theory; the inset zooms into the low-bias section. The mismatch between theory and experiment at negative potential drop eV is partly due to the absence of the contribution from the $\mu_R = \mu(2)$ Coulomb peak, which is not included in the KEA theory due to the assumption of an infinite charging energy.

* kensuke@meso.phys.sci.osaka-u.ac.jp

† milena.grifoni@physik.uni-regensburg.de

¹ Y. Meir and N. Wingreen, Phys. Rev. Lett. **68**, 2512 (1992).

² Y. Meir, N. Wingreen, and A. P. Lee, Phys. Rev. Lett. **70**, 2601 (1993).

³ N. S. Wingreen and Y. Meir, Phys. Rev. B **49**, 11040 (1994).

⁴ D. R. Schmid, S. Smirnov, M. Margańska, A. Dirnreichner, P. L. Stiller, M. Grifoni, A. K. Hüttel, and C. Strunk, Phys. Rev. B **91**, 155435 (2015).

⁵ A. Kamenev, *Field Theory of Non-Equilibrium Systems* (Cambridge University Press, 2011).

⁶ A. Altland and B. Simons, *Condensed Matter Field Theory* (Cambridge University Press, 2006).

⁷ S. Smirnov and M. Grifoni, Phys. Rev. B **87**, 121302 (2013).

⁸ D. C. Langreth, Phys. Rev. **150**, 516 (1966).

⁹ M.-S. Choi, R. López, and R. Aguado, Phys. Rev. Lett. **95**, 067204 (2005).

¹⁰ A. C. Hewson, *The Kondo Problem to Heavy Fermions*, Cambridge Studies in Magnetism (Cambridge University Press, 1993).

¹¹ R. Sakano and N. Kawakami, Phys. Rev. B **73**, 155332 (2006).

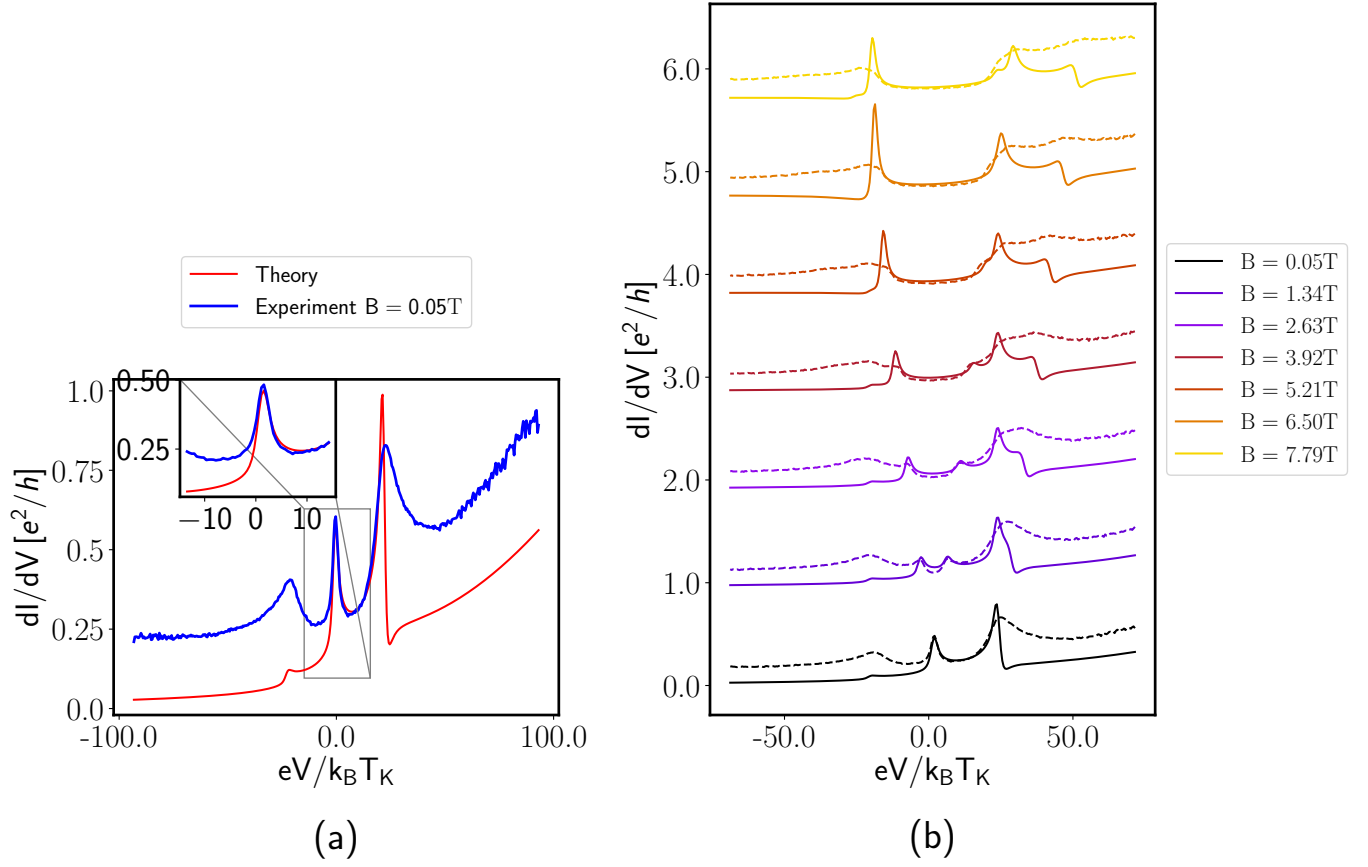
¹² D. Mantelli, C. Moca, G. Zaránd, and M. Grifoni, Physica E **77**, 180 (2016).

¹³ C. Mora, P. Vitushinsky, X. Leyronas, A. A. Clerk, and K. Le Hur, Phys. Rev. B **80**, 155322 (2009).

¹⁴ S. Smirnov and M. Grifoni, Phys. Rev. B **84**, 125303 (2011).

¹⁵ M. Pletyukhov and H. Schoeller, Phys. Rev. Lett. **108**, 260601 (2012).

¹⁶ C. W. J. Beenakker, Phys. Rev. B **44**, 1646 (1991).



Supplementary Figure S-8: Differential conductance for the $N = 3$ case, at (a) $B = 0.05$ T and (b) for various values of the magnetic field. The blue curve in (a) shows the experimental data while the red curve is the result of the KEA theory; the inset zooms into the low-bias section. The discrepancy at positive bias drop is partly due to the absence of the $\mu(3) = \mu_R$ Coulomb peak in the KEA theory due to the assumption of infinite charging energy.